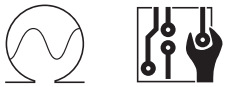

Technische Universität München
TUM School of Computation, Information and Technology
Institute for Electronic Design Automation

Stochastic Optimization for Wavelength-Routed Optical Network-on-Chips Design under Process Variation

Master Thesis

Liaoyuan Cheng

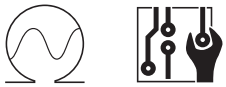

Technische Universität München
TUM School of Computation, Information and Technology
Institute for Electronic Design Automation

Stochastic Optimization for Wavelength-Routed Optical Network-on-Chips Design under Process Variation

Master Thesis

Liaoyuan Cheng

Supervisor :	Dr.-Ing. Tsun-Ming Tseng
Supervising Professor :	Prof. Dr. Martin Schottenloher, Prof. Dr.-Ing. Ulf Schlichtmann
Topic issued :	07.03.2023
Date of submission :	29.08.2023

Liaoyuan Cheng
Ludwig-Maximilians-Universität München
Master Mathematics

Abstract

Wavelength-Routed Optical Network-on-Chip (WRONoC) possesses the advantages of high bandwidth and low latency and holds substantial potential to meet the escalating communication demands of multi-core processors. In WRONoC, all signal transmission paths are preserved during the design phase of the communication topology, which enables simultaneous, collision-free signal communications among all initiators and targets. The key optical components for signal routing include waveguides, and a ring-shaped waveguide called a micro-ring resonator (MRR). The optical path length of the MRR is calculated based on its radius. When the optical path length of the MRR is an integer multiple of the signal wavelength, the MRR can resonate with the signal and change its transmission direction; otherwise, the signal is transmitted in the original direction. It is worth noting that high-refractive-index contrast materials used to fabricate the MRRs are susceptible to process variation, which can lead to changes in the MRR radius. Such changes will shift the power transmission spectrum of the MRR with respect to wavelength and cause unexpected power loss. This reduces the signal power arriving at the destination, and the crosstalk increases. When process variation occurs in more than one MRR, crosstalk effects accumulate and severely degrade signal transmission quality in the network.

Previous topology designs did not consider these effects caused by process variation. To overcome these challenges, I first quantify the signal transmission power when the MRR suffers process variation. Then, I build a mathematical model and develop a stochastic optimization algorithm that can optimize the expected signal transmission power of different WRONoC topologies under process variation. Experimental results show that this optimization approach is applicable to a variety of WRONoC topology designs and can significantly improve the expected signal transmission power when relative process variation occurs. As this process variation becomes greater, the effectiveness of the approach increases accordingly. Compared to the case where this variation is not considered, this approach can achieve up to more than twice the expected signal power transmission. This demonstrates the robustness of the approach against process variation.

Acknowledgements

Firstly, I want to thank Prof. Dr. Martin Schottenloher for giving me the opportunity and support to complete this master's thesis.

Secondly, I want to give special thanks to Dr.-Ing. Tsun-Ming Tseng. His support and guidance have been invaluable to me.

Lastly, I want to express my heartfelt thanks to my family, who consistently supported and encouraged me.

Contents

List of Figures

List of Tables

1. Introduction

A multiprocessor system-on-chip (MPSoC) is a highly integrated chip widely used in microcontrollers or systems-on-a-chip that require high processing power. As the demand for data transmission within MPSoCs increases, achieving high-performance inter-core communication has become a major challenge.

Traditional electronic networks-on-chips (NoCs) may not be able to support the coming demands for performance and power due to bandwidth limitations and the high power consumption of metal interconnects (Ye et al. 2009). With the development of silicon photonics, optical networks-on-chip (ONoC) are becoming an effective solution to the limitations of electronic NoCs. By using wavelength-division multiplexing (WDM) technology, ONoCs enable a single waveguide to carry multiple optical signals on different wavelengths, providing on-chip communication with high bandwidth and low signal latency (Tseng et al. 2019).

There are two main types of ONoCs: 1) active networks that require a control layer to employ real-time switching mechanisms for routing processes, and 2) passive networks that utilize routing components resonating at distinct wavelengths (Truppel et al. 2020). Of these, wavelength-routed optical networks-on-chips (WRONoCs) fall into the latter category, where the data transmission path is entirely determined by its sender and wavelength, and routing elements such as waveguide and silicon micro-ring resonators (MRR), where the MRR consists of a looped waveguide, are used to deliver the signal to its destination. Active networks require a control layer to dynamically establish signal paths. In contrast, all signal paths are statically preserved during the design phase of WRONoC, which allows all initiators and targets to communicate simultaneously without data collision and eliminates the dynamic overhead of the control layer (Truppel et al. 2020).

In WRONoC systems, optical signals are transmitted through waveguides and can be turned by coupling to MRRs. The degree of coupling between the signal and the MRR depends on the radius of the MRR and the wavelength of the signal. In particular, if the optical path

circumference of the MRR is an integer number of the wavelength of the signal, then the signal is maximally coupled to the MRR, a condition also referred to as being "on-resonance" with the MRR. An MRR can resonate with multiple wavelengths, and these wavelengths are referred to as "resonant wavelengths" of this MRR. If this condition is not satisfied, the signal is only partially coupled to the MRR (Bogaerts et al. 2012). Wavelengths that meet this latter condition are called "non-resonant wavelengths" of this MRR. I illustrate this coupling mechanism using an example shown in Figure 1.1. The red and blue lines represent optical signals of different wavelengths that are resonant wavelengths of the same colored MRRs. When two optical signals enter this simplified network from the initiator I_1, the red signal first encounters an MRR that resonates with it and is directed toward the target T_1. Simultaneously, the red MRR does not resonate with the blue signal, so the blue signal maintains its original transmission direction until it encounters a blue MRR. The blue MRR resonates with it and turns it towards target T_2. Thus, through this coupling mechanism, the red signal is transmitted from I_1 to T_1, and the blue signal is transmitted from I_1 to T_2.

During the signal transmission process, power loss occurs when the signal passes through waveguide intersections and couples with the MRR. This loss, known as insertion loss, can affect the overall efficiency of the transmission. Transmission efficiency is specifically defined as the ratio of the signal's transmitted power at the designated location to its original input power. Several advanced WRONoC topologies have been suggested, including the λ-router (Brière et al. 2007), GWOR (Tan et al. 2011), Snake (Ramini et al. 2013), Light (Zheng et al. 2021) and CustomTopo (Li et al. 2018). These topology designs are aimed at minimizing insertion loss to meet signal communication requirements. This can be achieved by adjusting the position of MRRs, reducing the number of MRRs and wavelengths, and optimizing waveguide routing, among other strategies. However, the design of these topologies has not taken into consideration the impact of process variation on WRONoC. Process variation, a phenomenon occurring during manufacturing, leads to changes in the radius of the MRR. As a result, the transmission

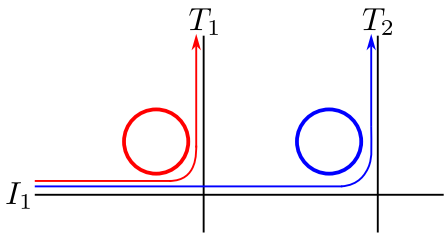

Figure 1.1.: Example of optical signal coupling mechanism to MRR.

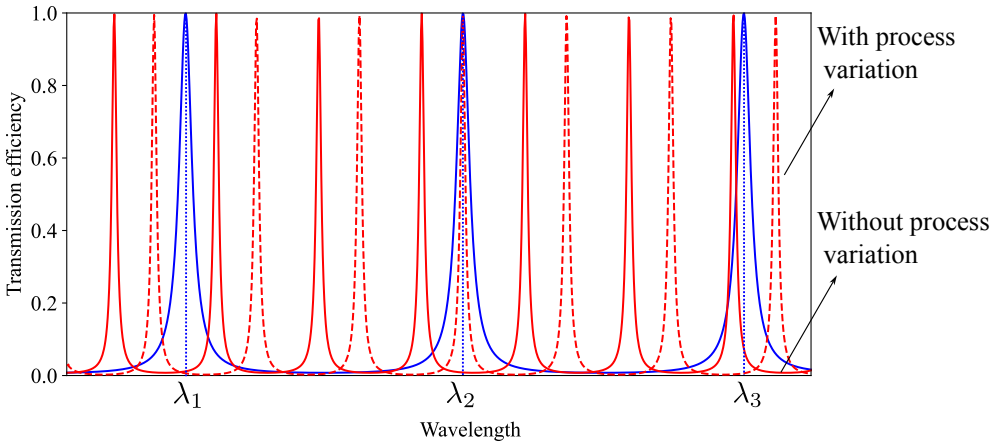

Figure 1.2.: Transmission efficiency spectra for red and blue MRRs with and without process variation.

efficiency spectrum of the MRR shifts (Mirza et al. 2020). This shift leads to significant power insertion loss and crosstalk in the network, as illustrated in Figure 1.2. The red and blue solid curves in Figure 1.2 represent the transmission efficiency spectra with respect to different wavelengths of the same colored MRR without process variation in Figure 1.1. The wavelengths corresponding to the peaks of these curves are the resonant wavelengths for the MRR, while the wavelengths at the troughs are the non-resonant wavelengths. In order to transmit a signal from I_1 to T_2 in Figure 1.1, the resonant wavelength of the blue MRR can be chosen along with the non-resonant wavelength of the red MRR. Wavelengths λ_1, λ_2, and λ_3 all satisfy these conditions. When the red MRR suffers process variation, its transmission efficiency spectrum shifts, as shown by the red dashed curve. This causes λ_2 to become a resonant wavelength for both the red and blue MRRs. If λ_2 is chosen as the resonant wavelength for the blue signal traveling from I_1 to T_2, the blue signal will first encounter the red MRR and be on-resonance with it, redirecting to T_1. The misdirected blue signal to T_1 becomes crosstalk noise in the communications network. Meanwhile, the intended target T_2 receives little or none of the blue signal's power, resulting in significant power insertion loss. Although more than one wavelength can be selected for the signal to resonate with an MRR, this example shows that not every resonant wavelength is the optimal choice when the signal passes through multiple MRRs with process variation. Therefore, it is important to fully investigate the expected changes in the transmission efficiency spectrum with this variation. Based on this understanding, the selection of signal wavelengths and MRR radii should be optimized to ensure that the communication requirements are met.

In this thesis, I identify shortcomings in existing research and propose a stochastic optimization method. By using the expected value as a key metric to evaluate system performance under process variation, this method aims to maximize the expected value of signal transmission efficiency (also referred to as the expected transmission efficiency) by optimizing the selection of MRR radii and signal wavelengths. I begin by introducing the WRONoC's background and exploring the causes of process variation in Chapter 2. Next, Chapter 3 includes a review of the models in (Bogaerts et al. 2012) and (Chrostowski & Hochberg 2015) that calculate transmission efficiency based on MRR radius and signal wavelength. This chapter also details the impact of process variation on WRONoC, reviews previous work in this area, highlights the limitations of the state-of-the-art in addressing the issues under study, and formalizes the problem definition for optimizing the expected transmission efficiency. In Chapter 4, I combine the transmission efficiency models with probability theory, construct analytical models for the expected transmission efficiency under process variation, and use the results as design options for optimization. Then, I build an integer-linear programming (ILP) model to provide an exact optimization solution. Since the complexity of the ILP problem is NP-hard, it becomes increasingly difficult to find a solution in a feasible time as the problem size increases. To overcome this limitation, I develop a simulated annealing algorithm tailored for WRONoC properties, which is a stochastic optimization algorithm that efficiently provides approximate solutions in a faster feasible time with more design options than ILP. All the optimization methods are detailed in Chapter 5. I further present the experimental setup and analyze the results in Chapter 6. The thesis concludes in Chapter 7, where I summarize the main findings and suggest potential directions for future research.

2. Wavelength-Routed Optical Network on Chip

This chapter presents the fundamentals of WRONoC. First, the representative experimental setting for WRONoC is explored. Next, the routing elements that constitute WRONoC are introduced. After that, the logical designs of different WRONoC routers are described. Finally, the insertion loss and fabrication process variations are discussed.

2.1. Experimental Setup for WRONoC

The experimental environment of the WRONoC is based on the 3D-structure shown in Figure 2.1, which consists of a multi-core processor, an electronic layer, and a vertically aligned photonic layer (Tseng et al. 2019). In the electronic layer, multiple processor cores are organized into clusters, each with its own hub, and these hubs are connected to the photonic layer by through-silicon vias (TSVs) (Tseng et al. 2019). The off-chip laser sources generate light of different wavelengths (Ramini et al. 2013). These wavelengths enter the power distribution network and are routed to the electrical/optical (E/O) interface. At this interface, with the provided wavelengths, the data from the original electrical signals are converted to optical signals (Tseng et al. 2019). Finally, these optical signals are passively transmitted by the WRONoC router through the waveguide to each communication node in the network. This router specifies the initiator and target of the optical signal transmission and defines the path of the optical signal for data transmission (Tseng et al. 2019), and enables communications (1) between hubs; (2) from a hub to an off-chip memory controller; and (3) from a memory controller to a hub (Ramini et al. 2013). If the received optical signals need to be processed or read, they are converted back to electrical signals at the optical/electrical (O/E) interface (Tseng et al. 2019). These electrical signals can then be processed.

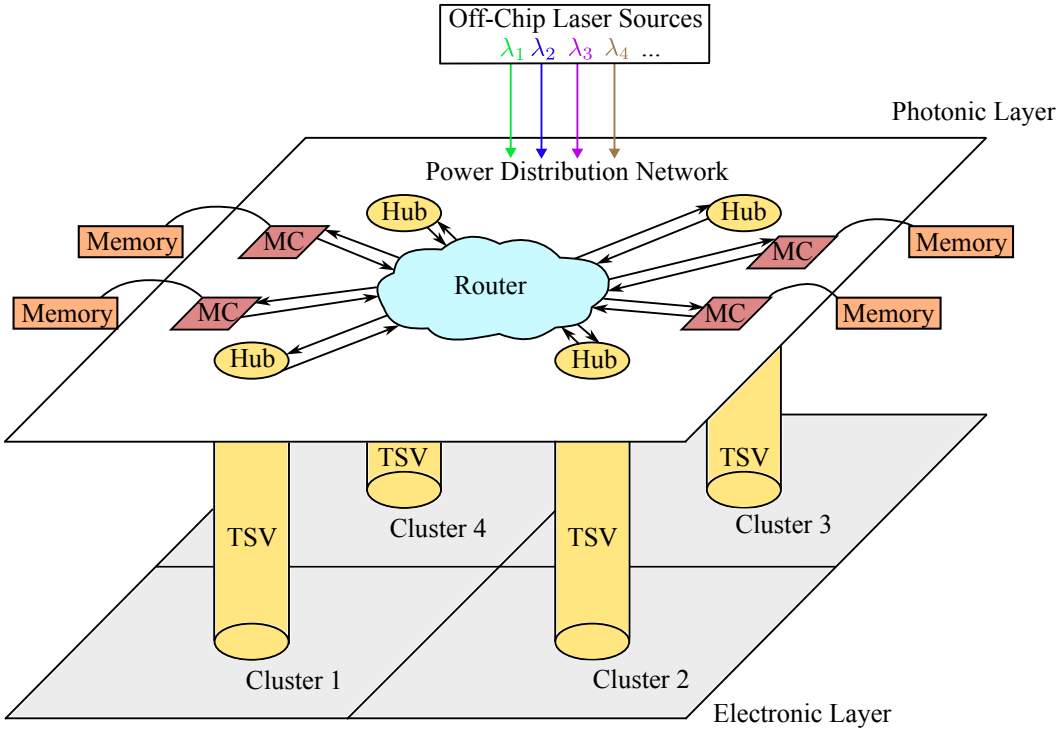

Figure 2.1.: A representative experimental setup for WRONoC on a 3D-structured chip.

2.2. Routing Elements

Waveguide serves as physical channels for optical signal transmission, and MRR is a critical component for modulating and directing optical signals. Together, they form the backbone of the WRONoC system. A detailed discussion of their structure and functionality is presented in this section.

2.2.1. Optical Waveguide

As the fundamental elements of photonic devices, waveguides are responsible for signal transmission and connecting diverse photonic components. An optical waveguide is a planar dielectric structure consisting of a cladding material surrounding a core (Nakagawa et al. 2001). In this work, a silicon-insulator (SOI) material is used for the optical waveguide. Figure 2.2 shows the structure of a SOI waveguide section (Mohammed et al. 2021). The optical waveguide is

specially designed to use a silicon core formed on an insulating silicon substrate with its own height and width (Chrostowski & Hochberg 2015). The silicon core is then covered by the cladding of an insulator (usually silicon oxide), which takes advantage of the high refractive index difference between silicon and insulator to achieve controlled propagation of the optical signal inside the silicon core (Bogaerts et al. 2012).

Such silicon optical waveguides are typically fabricated using e-beam or optical lithography techniques in combination with reactive ion etching, operations typically performed on CMOS fabrication tools (Bogaerts et al. 2012). With improvements in process technology, the propagation loss of silicon conductors can be reduced to less than 3 dB/cm (Bogaerts et al. 2012). Several optical signals on different wavelengths can be transmitted through the same optical waveguide without interference, achieving high bandwidth for optical waveguide transmission, which is called wavelength division multiplexing (WDM) technology (Li et al. 2018).

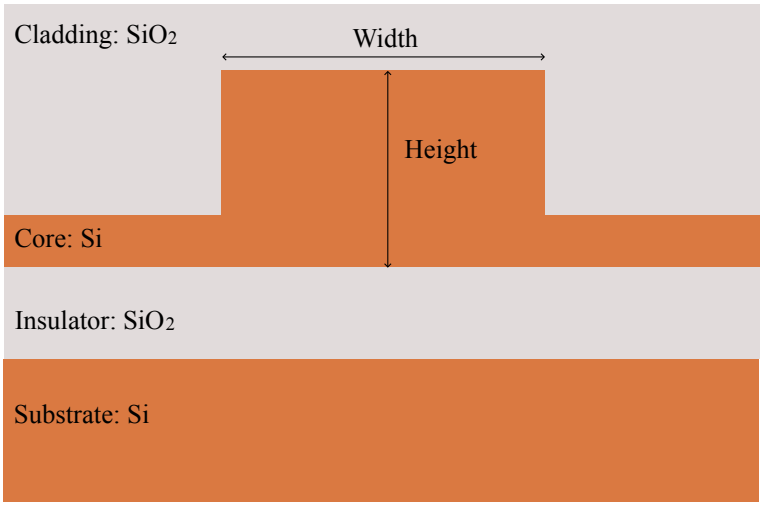

Figure 2.2.: SOI waveguide section.

2.2.2. Micro-Ring Resonator

Micro-ring resonators (MRRs) are composed of ring-shaped waveguides that operate using a coupling mechanism. The situation of a signal passing through an MRR can be divided into two cases: on-resonance and off-resonance, according to the radius of the MRR (Bogaerts et al. 2012). The signal enters the MRR through the input port, and if the optical path length

of the MRR is exactly an integer number of wavelengths, then the signal is on-resonance with the MRR (Bogaerts et al. 2012). The signal is off-resonance with the MRR if this condition is not met (Bogaerts et al. 2012).

There are two types of MRR: all-pass MRR and add-drop MRR. As shown in Figure 2.3, an all-pass MRR operates by coupling to a single waveguide with an input and a through port. When optical signals of two different wavelengths, λ_1 and λ_2, enter the all-pass MRR from the input port, distinct paths are taken. The signal on λ_1, indicated by the blue line, is on-resonance with the ring, causing it to travel along the ring and then return back into the waveguide, finally out of the through port. The signal on λ_2, indicated by the green line, is off-resonance with the ring, travels directly along the waveguide, and finally outputs from the through port as well. Thus, an all-pass MRR can allow all wavelengths of signals to pass through the device and adjust the phase of the optical signal without affecting the amplitude spectrum of the signal (Chen et al. 2022), but it does not have the ability to filter wavelength-specific optical signals.

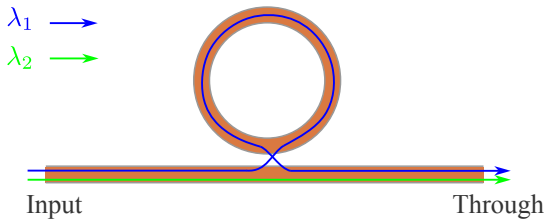

Figure 2.3.: All pass MRR.

On the other hand, the add-drop MRR works by coupling to two waveguides. It has four ports: an input port, a through port, an add port, and a drop port. There are two structures that can be used to change the direction of signal transmission and achieve the filtering function of different wavelengths. One is the parallel switching element (PSE) structure, as shown in Figure 2.4, in which two waveguides are placed in parallel at the top and bottom of the ring structure. The optical signals of two different wavelengths, λ_1 and λ_2, enter the add-drop MRR from the input port. The signal on λ_1, indicated by the blue line, is on-resonance with the ring so that the optical signal travels around the ring and is rotated 180 degrees. After coupling to the top waveguide, it exits through the drop port. Conversely, the signal on λ_2, indicated by the green line, is off-resonance with the ring and maintains its propagation direction in the bottom waveguide, finally exiting the through port. The other is the cross switching element (CSE) structure, where the waveguides are crossed orthogonally, and a ring is placed near the

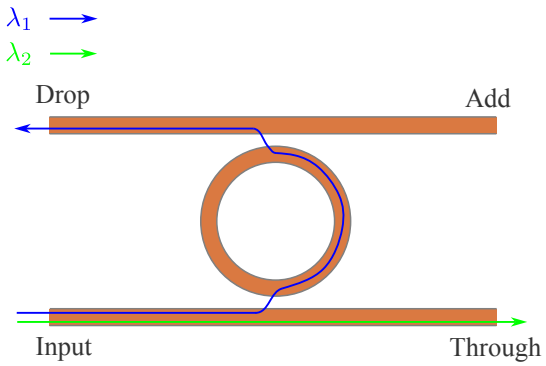

Figure 2.4.: PSE structure with 180 degrees rotation.

crossing waveguides. Figure 2.5 (a) shows that the signal on wavelength λ_1, indicated by the blue line, enters the add-drop MRR from the input port and is on-resonance with the ring. The signal is then rotated 90 degrees to couple to the other waveguide and output from the drop port. The signal on wavelength λ_2, indicated by the green line, is off-resonance with the ring, so the signal continues to travel in the waveguide and is finally output from the through port. Similarly, Figure 2.5 (b) shows that the signal on wavelength λ_1, indicated by the blue line, enters the add-drop MRR from the input port and is on-resonance with the ring. The signal is then turned 270 degrees and coupled to the other waveguide and output from the drop port. The signal on wavelength λ_2, indicated by the green line, is off-resonance with the ring, so the signal keeps its traveling direction and is finally output from the through port. In both cases, the add-drop MRR provides filtering and routing of the optical signals on specific wavelengths. Therefore, unless otherwise noted, every mention of MRR in this work refers to add-drop MRR.

Depending on the signal routing requirements, if the signal is designed to be transmitted to the drop port of the MRR, the MRR is called the **drop MRR** for that signal. Conversely, if the signal is designed to be transmitted to the through port of the MRR, the MRR is called the **through MRR** for that signal.

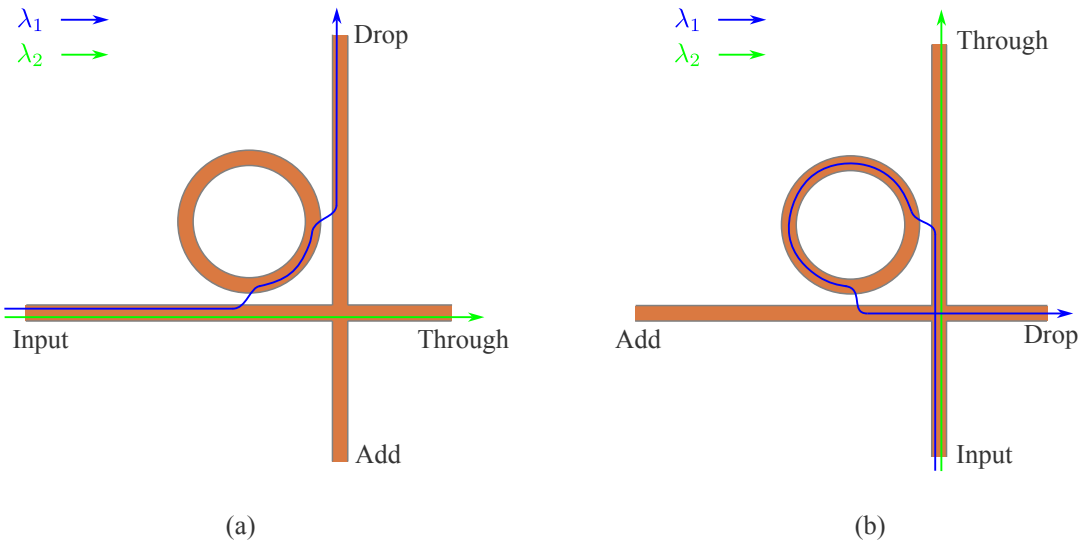

Figure 2.5.: (a) CSE structure with 90 degrees rotation. (b) CSE structure with 270 degrees rotation.

2.3. Logical Design of Router

To achieve communication between different cores (hubs or memories) in Figure 2.1, researchers have constructed two main types of logical topology designs: full-connectivity topology and application-specific topology. In this work, the core initiating the signal is referred to as the **master**, while the target core receiving the signal is referred to as the **slave**.

2.3.1. Full-Connectivity Topologies

In the full-connectivity topology, each core has a path for signal transmission with other cores. Representative examples include the following and are illustrated in Figure 2.6:

λ-router: The λ-router is proposed in (Brière et al. 2007). It is necessary to use CSE structures with $N \times (N-1)$ MRRs to achieve a complete N-cores-to-N-cores connection. A λ-router is shown in Figure 2.6 (a) with four masters (m_1, m_2, m_3, m_4) connected to four slaves (s_1, s_2, s_3, s_4) using 12 MRRs.

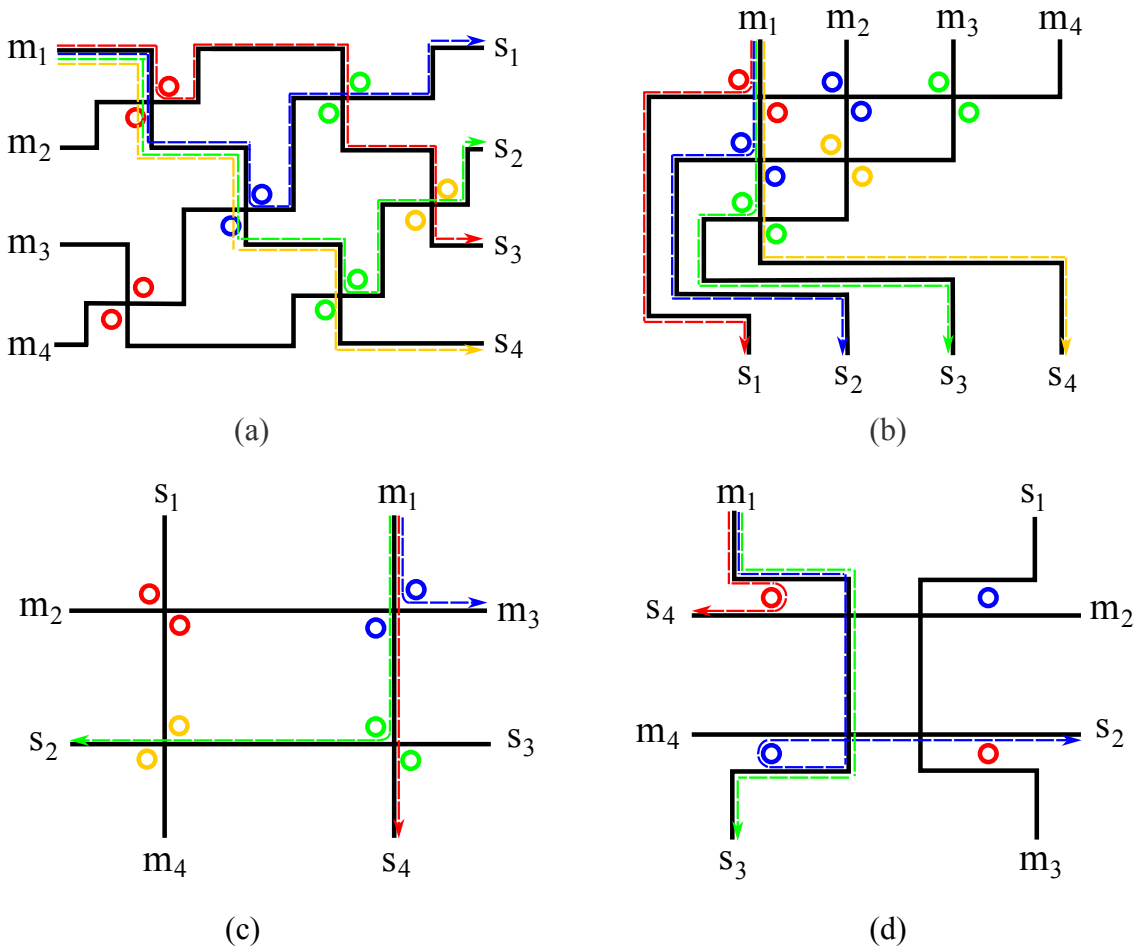

Figure 2.6.: (a) 4×4 λ-router. (b) 4×4 Snake. (c) 4×3 GWOR. (d) 4×3 Light.

Snake router: The Snake-router is proposed in (Ramini et al. 2013). It is necessary to use CSE structures with $N \times (N-1)$ MRRs to achieve a complete N-cores-to-N-cores connection. A Snake-router is shown in Figure 2.6 (b) with four masters connected to four slaves using 12 MRRs.

GWOR: The generic wavelength-routed optical router (GWOR) proposed by (Tan et al. 2011) interconnects N cores and requires the CSE structures with $N \times (N-2)$ MRRs. This topology does not support self-communication, i.e., each core cannot communicate with itself but can communicate with other cores. Figure 2.6 (c) shows the communication structure of four masters with four slaves.

Light: The Light-router is presented in (Zheng et al. 2021), which requires PSE structures with $2\lceil\frac{N}{2}\rceil(\lceil\frac{N}{2}\rceil - 1)$ MRRs to achieve connectivity between N cores. Similar to the GWOR, the Light-router does not support self-communication. Figure 2.6 (d) shows the topology of a Light-router connecting four cores.

In Figure 2.6, MRRs that can resonate with the same wavelengths are shown with the same color. Each topology design then shows the conflict-free signal transmission path from m_1 to each slave with different colored dashed lines. When a signal encounters an MRR of the same color, resonance occurs, and the propagation direction of the signal is changed.

2.3.2. Application-Specific Topologies

Application-specific topologies provide tailored connectivity where nodes without data transmission requirements are not interconnected. Topologies synthesized through such a design automation approach are proposed in previous work: CustomTopo (Li et al. 2018), PSION+ (Truppel et al. 2020) and FAST+ (Xiao et al. 2022).

2.4. Insertion Loss

During the signal transmission process, the signal power is affected by various types of loss, referred to as insertion loss. These include **propagation loss**, which occurs as the signal is transmitted through the waveguide; **crossing loss**, which occurs when the signal traverses crossing optical waveguides; **bending loss**, which happens when the signal is transmitted along the waveguide in a bend; **drop loss** occurs when the signal is resonant with the MRR; and **through loss**, which occurs when signals pass through MRR without resonating.

2.5. Process Variation

The manufacturing process for ONoC devices generally begins on CMOS manufacturing tools with the preparation of a silicon-on-insulator (SOI) wafer. This wafer is composed of three

layers, namely a thin silicon layer, an insulating layer, and a silicon substrate, as shown in Figure 2.2. Wafer-level processing techniques, such as cladding deposition, chemical-mechanical polishing, baking, and etching, are employed to fabricate the necessary structures. At the chip level, UV lithography is used to pattern waveguides, MRRs, and other optical components (Selvaraja et al. 2010), and then the exposed silicon is removed by wet or dry etching to create the required structure (O'Connor et al. 2012).

Process variation in WRONoC occurs primarily due to the lithography and etching imperfections of devices. They can be caused by factors including poor mask pattern quality, lithography limitations, equipment inaccuracies in etch depth and deposition rate, as well as environmental influences such as tuning temperature and input power. These variations can occur randomly or systematically over time and space (Selvaraja et al. 2010). In particular, this work considers only the irreversible process variations that occur during manufacturing and does not take into account modifiable environmental factors.

3. Problem Description

This chapter first establishes the power transmission efficiency models for the MRR and the signal. Then, based on these models, the challenges posed by process variations are illustrated. Next, related works that attempt to address these challenges are reviewed, and the limitations of the state of the art are discussed. Finally, the optimization problem that this work aims to solve is defined.

3.1. Transmission Efficiency Model

Based on the MRR radius and signal wavelength, I formulate the signal transmission efficiency at the drop port and through port of a single MRR. The parameters and formulas are reviewed from (Bogaerts et al. 2012) and (Chrostowski & Hochberg 2015) if not otherwise specified. The parameters that appear in Figure 3.1 and Figure 3.2, as well as other required parameters for the models, are introduced below:

S_{input}: The signal input power intensity.

S_{drop}: The signal power intensity at the drop port of the MRR.

S_{through}: The signal power intensity at the through port of the MRR.

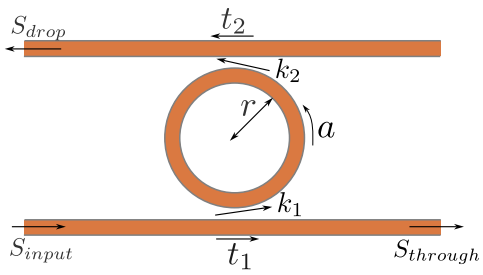

Figure 3.1.: PSE structure with coupling parameters.

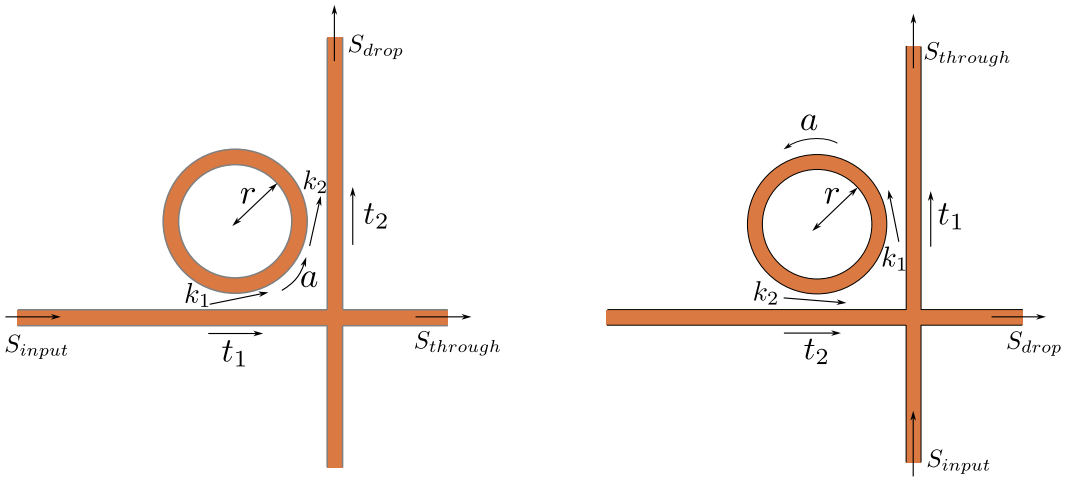

Figure 3.2.: CSE structure with coupling parameters.

r: The radius of the MRR.

L_r: The optical round-trip path length of the MRR.

λ: The wavelength of the signal.

$n_{\text{eff}}(\lambda)$: The effective refractive index on wavelength λ in the SOI waveguide.

$\beta(\lambda)$: The propagation constant of the circulating mode.

$\phi(r, \lambda)$: The phase shift.

a: The single-pass amplitude transmission, which characterizes the losses in the MRR due to factors such as propagation and bending losses. In this work, such losses are assumed to be ignored, and consequently, a is set equal to 1, i.e., $a = 1$.

k_1, k_2, k: The cross-coupling coefficients, which represent the portion of the input power that is coupled from one waveguide to the other. In this work, a symmetric coupling scenario is assumed, and the cross-coupling coefficients are set accordingly as $k_1 = k_2 = k \in [0, 1]$.

t_1, t_2, t: The self-coupling coefficients, which represent the portion of the input power that remains in the waveguide after the interaction with other waveguide. In this work, the self-coupling coefficients are set as $t_1 = t_2 = t \in [0, 1]$.

$H_{\text{drop}}(r, \lambda)$: The transmission efficiency function of a signal, on a wavelength of λ, at the drop port of an MRR with a radius of r.

$H_{\text{through}}(r, \lambda)$: The transmission efficiency function of a signal, on a wavelength of λ, at the

through port of an MRR with a radius of r.

Given the wavelength of the signal, the radius of the MRR, and the cross-coupling coefficient, these parameters can be calculated as follows:

$$n_{\text{eff}}(\lambda) = 2.57 - 0.85(\lambda[\mu m] - 1.55) \tag{3.1}$$

$$\beta(\lambda) = \frac{n_{eff}(\lambda)2\pi}{\lambda} \tag{3.2}$$

$$\phi(r, \lambda) = \beta(\lambda)2\pi r \tag{3.3}$$

$$t^2 = 1 - k^2 \tag{3.4}$$

From Equation (3.2) and Equation (3.3), it can be concluded that the larger the radius of the MRR, the greater the number of wavelengths that can resonate. This is because as the radius of the MRR increases, the length of the optical path that must travel within the MRR increases accordingly. Thus, more wavelengths can satisfy the same phase shift condition.

By employing the given equations, the transmission efficiency functions of a signal, on a wavelength of λ, at the drop port and through port of an MRR with a radius of r can be determined as below:

$$\begin{aligned} H_{\text{drop}}(r, \lambda) &= \frac{S_{\text{drop}}}{S_{\text{input}}} \\ &= \frac{(1-t^2)(1-t^2)a}{1 - 2t^2 a cos(\phi(r, \lambda)) + (t^2 a)^2} \\ &= \frac{k^2 k^2 a}{1 - 2t^2 a cos(\phi(r, \lambda)) + (t^2 a)^2} \\ &\overset{a=1}{=} \frac{k^4}{1 - 2t^2 cos(\phi(r, \lambda)) + (t^2)^2} \end{aligned} \tag{3.5}$$

$$H_{\text{through}}(r, \lambda) = \frac{S_{\text{through}}}{S_{\text{input}}}$$

$$
\begin{aligned}
&= \frac{t^2a^2 - 2t^2a\cos(\phi(r,\lambda)) + t^2}{1 - 2t^2a\cos(\phi(r,\lambda)) + (t^2a)^2} \\
&= \frac{t^2(a^2+1) - 2t^2a\cos(\phi(r,\lambda))}{1 - 2t^2a\cos(\phi(r,\lambda)) + (t^2a)^2} \\
&\overset{a=1}{=} \frac{2t^2 - 2t^2\cos(\phi(r,\lambda))}{1 - 2t^2\cos(\phi(r,\lambda)) + (t^2)^2}
\end{aligned} \tag{3.6}
$$

Using the condition $t^2 + k^2 = 1$, $H_{\text{through}}(r,\lambda)$ can be written as:

$$
\begin{aligned}
H_{\text{through}}(r,\lambda) &= \frac{S_{\text{through}}}{S_{\text{input}}} \\
&\overset{a=1}{=} \frac{2t^2 - 2t^2\cos(\phi(r,\lambda))}{1 - 2t^2\cos(\phi(r,\lambda)) + (t^2)^2} \\
&= \frac{t^2 + (1-k^2) - 2t^2\cos(\phi(r,\lambda))}{1 - 2t^2\cos(\phi(r,\lambda)) + (t^2)^2} \\
&= \frac{(t^2-k^2) + 1 - 2t^2\cos(\phi(r,\lambda))}{1 - 2t^2\cos(\phi(r,\lambda)) + (t^2)^2} \\
&= \frac{(t^2+k^2)(t^2-k^2) + 1 - 2t^2\cos(\phi(r,\lambda))}{1 - 2t^2\cos(\phi(r,\lambda)) + (t^2)^2} \\
&= \frac{t^4 - k^4 + 1 - 2t^2\cos(\phi(r,\lambda))}{1 - 2t^2\cos(\phi(r,\lambda)) + (t^2)^2} \\
&= 1 - \frac{k^4}{1 - 2t^2\cos(\phi(r,\lambda)) + t^4} \\
&= 1 - H_{\text{drop}}(r,\lambda)
\end{aligned} \tag{3.7}
$$

It is now possible to construct a model for the transmission efficiency of the signal sent by the master and received by the slave. Since propagation loss and bending loss are related to the physical layout design and cannot be directly applied to the logical topology, these two losses will be ignored in this work.

I first introduce the following symbols to represent the expressions needed in the model:

$\mathcal{M}$: The set of masters, with $|\mathcal{M}|$ representing the total number of masters.

$\mathcal{S}$: The set of slaves, with $|\mathcal{S}|$ denoting the total number of slaves.

$\mathcal{SP}$: The set of all signals within the topology, with $|\mathcal{SP}|$ denoting the total number of signals.

(m_i, s_j): The signal sent by the i-th master m_i and received by the j-th slave s_j, where $i \in |\mathcal{M}|$, $j \in |\mathcal{S}|$ and $(m_i, s_j) \in \mathcal{SP}$.

cl: The coefficient of crossing loss, with cl_{dB} denoting the coefficient of crossing loss in dB.

$c_{(m_i,s_j)}$: The number of waveguide crossings in the transmission path of signal (m_i, s_j).

$\mathcal{MRR}$: The set of MRRs within the topology, with $|\mathcal{MRR}|$ denoting the total number of MRRs.

$\mathcal{MRR}_{(m_i,s_j)}$: The set of MRRs in the transmission path of signal (m_i, s_j), with $\mathcal{MRR}^{\text{drop}}_{(m_i,s_j)}$ denoting the set of drop MRRs in the transmission path of signal (m_i, s_j) and $\mathcal{MRR}^{\text{through}}_{(m_i,s_j)}$ denoting the set of through MRRs in the transmission path of signal (m_i, s_j).

mrr_h: The h-th MRR in the given topology.

Using these symbols, I then define the transmission efficiency model of the signal sent by the master and received by the slave without process variation:

Definition 3.1. Let $m_i \in \mathcal{M}$ and $s_j \in \mathcal{S}$. The transmission efficiency of signal (m_i, s_j), denoted by $H_{(m_i,s_j)}$, is defined as:

$$H_{(m_i,s_j)} = (1-cl)^{c_{(m_i,s_j)}} \prod_{mrr_h \in \mathcal{MRR}^{\text{drop}}_{(m_i,s_j)}} H_{\text{drop}}(r_x, \lambda_l) \prod_{mrr_f \in \mathcal{MRR}^{\text{through}}_{(m_i,s_j)}} H_{\text{through}}(r_y, \lambda_l). \quad (3.8)$$

Here, λ_l is the signal wavelength, and r_x, r_y are the radii of the mrr_h and mrr_f, respectively.

3.2. Process Variation Challenges

This work investigates the impact of process variation on the radius of MRR. Although state-of-the-art process technologies can achieve in-chip linewidth variations of less than 1% (Selvaraja et al. 2010)), it is notable that even a tiny process variation of 0.1% in radius can significantly

shift the transmission spectrum, which leads to signal power loss and crosstalk in the network. I explain this with the following example:

Example 3.2. The 4×3 Light-router shown in Figure 3.3 can be denoted as follows:

$$\mathcal{M} = \{m_1, m_2, m_3, m_4\};$$
$$\mathcal{S} = \{s_1, s_2, s_3, s_4\};$$
$$\mathcal{SP} = \{(m_1, s_2), (m_1, s_3), (m_1, s_4), \dots\};$$

In previous work, as shown in Figure 3.3, MRRs that resonate with the same wavelength

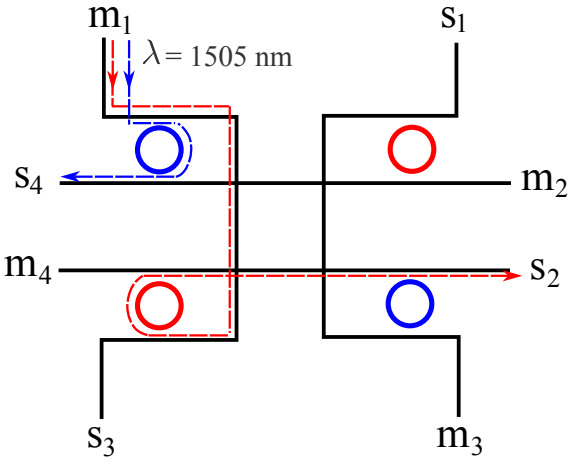

Figure 3.3.: The transmission path of signal (m_1, s_2) within a 4×3 Light topology.

are denoted by the same color. When a signal encounters an MRR, if a substantial portion of the signal can be transmitted into the drop port of the MRR, it's considered to be on-resonance. Conversely, if most of the signal is transmitted into the through port of the MRR, it's considered to be off-resonance.

To transmit a signal from m_1 to s_2, an appropriate red MRR radius and its resonant wavelength must be identified. I apply the signal transmission efficiency model at the drop port of the MRR with $k_1 = k_2 = 0.4$ (Li, Shen, Yu, Zhang, Chen & Zhang 2020) and plot the transmission spectra for radii of 10 μm and 27 μm within the 1500 nm – 1525 nm wavelength range in Figure 3.4. It can be seen that both radii can be chosen for red and blue MRRs. In the spectral curve, the wavelengths corresponding to the peaks represent the resonant wavelengths for each MRR, while those at the valleys can be considered non-resonant wavelengths. If I set

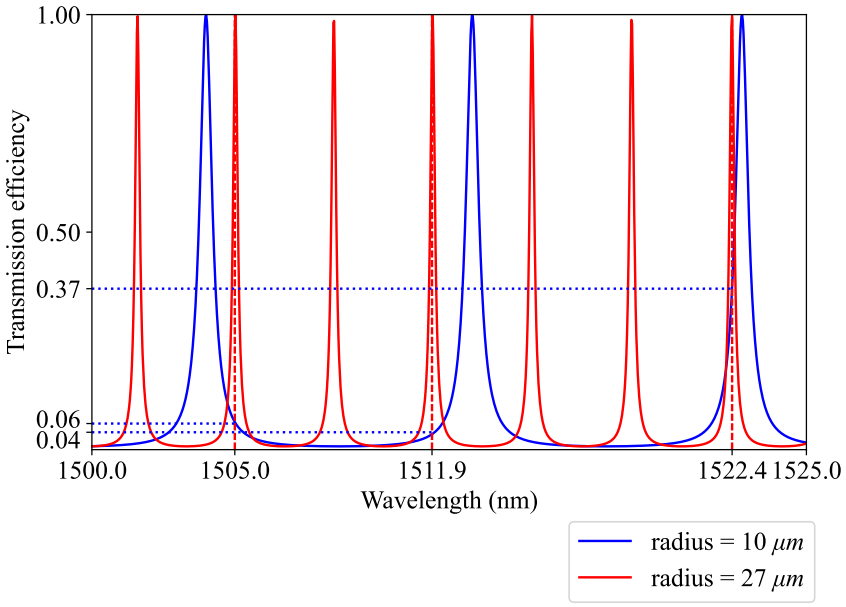

Figure 3.4.: Transmission spectra for MRRs with radii of 10 μm and 27 μm.

27 μm as the radius for the red MRR and 10 μm as the radius for the blue MRR, then the red MRR has seven resonant wavelengths, while the blue MRR has three resonant wavelengths. I select three resonant wavelengths of the red MRR, 1505 nm, 1511.9 nm, and 1522.4 nm, and calculate the transmission efficiency of the signal on these three wavelengths separately. I set the crossing loss to 0.009168 (Xiao et al. 2022) and consider four crossings in the transmission path of signal (m_1, s_2). The blue MRRs in the upper left and lower right corners are the "through MRRs" in this transmission path, while the red MRR in the lower left corner is the "drop MRR" in this transmission path. The transmission efficiency of the signal can be computed using the model in Definition 3.1. When considering 1522.4 nm as the signal wavelength, the transmission efficiency of signal (m_1, s_2) is calculated as

$$(1 - 0.009168)^4 \cdot (1 - 0.37) \cdot 1 \cdot (1 - 0.37) \approx 0.3825.$$

Less than 40% of the power can reach the receiving end s_2, which indicates that 1522.2 nm is unsuitable for a resonant wavelength under the given radii setting. The transmission efficiency of the signal on a wavelength of 1505 nm can be calculated as

$$(1 - 0.009168)^4 \cdot (1 - 0.06) \cdot 1 \cdot (1 - 0.06) \approx 0.8516.$$

Similarly, for the signal on a wavelength of 1511.9 nm, its transmission efficiency can be cal-

culated as

$$(1 - 0.009168)^4 \cdot (1 - 0.04) \cdot 1 \cdot (1 - 0.04) \approx 0.8883.$$

0.8516 and 0.8883 show that a significant amount of the signal can reach s_2. Both the 1505 nm and 1511.9 nm wavelengths can be resonant wavelengths of the red MRR, while they are non-resonant wavelengths of the blue MRR, positioning them as suitable wavelength choices for the signal (m_1, s_2).

Previous work overlooks the effect of process variation. Considering a process variation of 0.1% in the radius of the two MRRs, the radius of the red MRR changes to 10.01 μm, and the radius of the blue MRR changes to 27.027 μm. As a result, as shown in Figure 3.5, their transmission spectra shift. It can be seen that 1505 nm has become the resonant wavelength of the blue

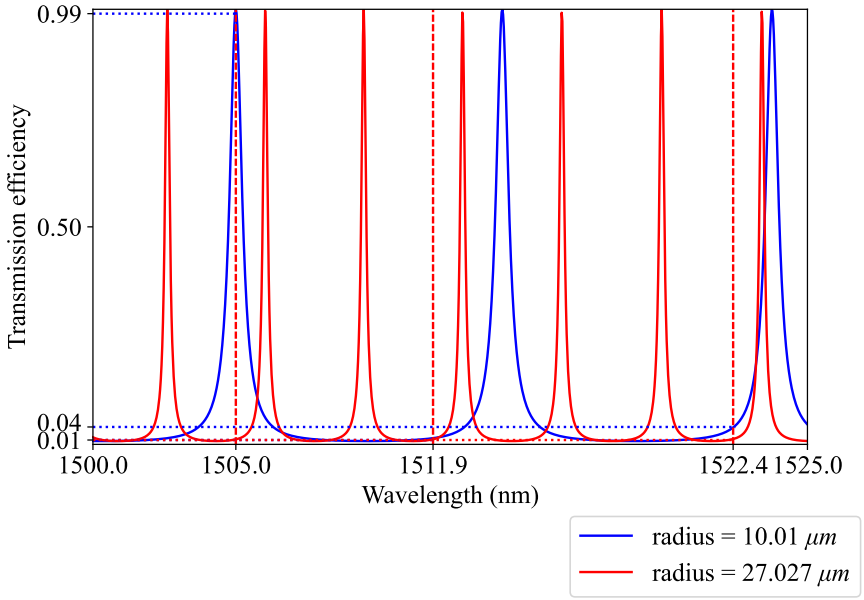

Figure 3.5.: Transmission spectra for MRRs with radii of 10.01 μm and 27.027 μm.

MRR. If 1505 nm is still chosen as the wavelength of signal (m_1, s_2), the transmission efficiency of this signal can be calculated as

$$(1 - 0.009168)^4 \cdot (1 - 0.99) \cdot 0.01 \cdot (1 - 0.99) \approx 0.000001.$$

This means that virtually no signal from m_1 can reach s_2. The insertion loss for this signal is massive, which requires more than one million times amplification of the laser power to

achieve the minimum power requirement at the receiving end. In addition, 99% of the signal is initially coupled to the first blue MRR and then transmitted to s_4. These signals, which should have been directed to s_2, become crosstalk noise, significantly reducing the signal-to-noise ratio at the s_4 port. It's important to note that any amplification of laser power will also correspondingly increase the crosstalk noise by the same factor. Similarly, the transmission efficiency of signal (m_1, s_2) on 1511.9 nm can be calculated as

$$(1 - 0.009168)^4 \cdot (1 - 0.01) \cdot 0.01 \cdot (1 - 0.01) \approx 0.0094.$$

Virtually no signal reaches s_2, which means massive signal insertion loss. Furthermore, the wavelength 1511.9 nm does not resonate with the changed red or blue MRR. Almost all the signal becomes crosstalk noise and is directly transmitted along the waveguide to slave s_3.

It can be seen that the previous designs of categorizing MRRs and signals based on communication requirements and resonance states are affected by process variation. In this work, to comprehensively investigate the options that are robust to process variation, I individually select the radius for each MRR as well as the wavelength for each signal. As shown in Figure 3.6, I label the MRR in the upper left corner as mrr_1, the MRR in the upper right corner as mrr_2, the MRR in the lower left corner as mrr_3, and the MRR in the lower right corner as mrr_4. Thus, the set of all MRRs in the topology can be given as follows:

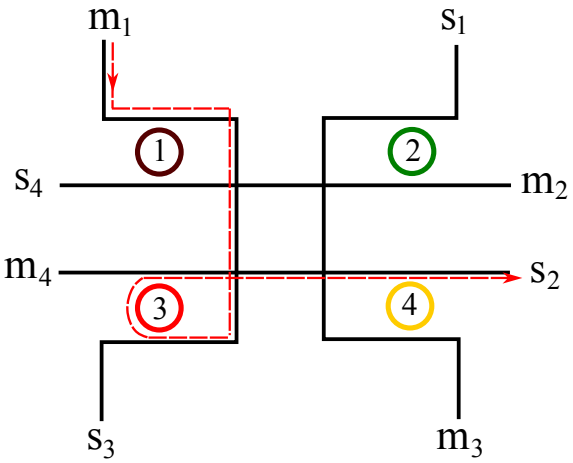

Figure 3.6.: The transmission path of (m_1, s_2) within a 4×3 Light topology with new denotations.

$$\mathcal{MRR} = \{mrr_1, mrr_2, mrr_3, mrr_4\}.$$

For example, The set of MRRs for different routing requirements in the transmission path of signal (m_1, s_2) can be described as

$$\mathcal{MRR}_{(m_1,s_2)} = \{mrr_1, mrr_3, mrr_4\};$$

$$\mathcal{MRR}^{\text{through}}_{(m_1,s_2)} = \{mrr_1, mrr_4\};$$

$$\mathcal{MRR}^{\text{drop}}_{(m_1,s_2)} = \{mrr_3\}.$$

Based on the topology structure, communication requirements, and process variation, I will determine the optimal combination of signal wavelengths and MRR radii to minimize insertion loss.

3.3. Related Works

There are several studies working on the methods to compensate for the impact of process variation in the ONoC integrating MRRs. The studies focus on two main directions: parameter optimization of MRR and enhancement of fault tolerance of ONoC systems.

In the domain of MRR parameter optimization, (Mirza et al. 2020) adjust the design parameters of MRR under process variation conditions, aiming to reduce the insertion loss as signal encounters the MRR. Similarly, (Weng et al. 2017) introduces a sparse combined generalized polynomial chaos (gPC) model for analyzing the uncertainty and optimizing the physical parameter design of a five-ring coupled resonator filter under process variation, thereby enhancing the robustness of the MRR to the process variation. The experiments of both studies are validated on a wavelength of 1550 nm. However, these two studies optimized parameters only for a specific signal wavelength and did not consider the more complicated scenarios in which an MRR may be passed by multiple signals simultaneously, and a signal may pass through multiple MRRs along its path. If the parameters of the MRR are optimized only for a specific signal wavelength, the transmission efficiency of other signals may be affected. Therefore, this work considers the communication requirements of WRONoC as well as the interaction effects between multiple signals and MRRs. Both MRR parameters and signal wavelengths are optimized in this work to improve the overall transmission efficiency of the network under process variation.

To improve the fault-tolerance of ONoC under process variation, (Meyer et al. 2015) proposed a fault-tolerant optical router with an electrical control module. However, this study is not applicable to WRONoC, which requires no control module. Considering the process variation that may occur in WRONoC, (Chuang et al. 2021) suggests adding backup MRRs to improve network reliability. However, this approach inevitably results in signals passing through additional MRRs, thereby increasing insertion loss.

In conclusion, this work is the first mathematical optimization method that requires no additional resource allocation and is universally applicable to various topological designs in WRONoC to maximize signal transmission efficiency and improve robustness under process variation.

3.4. Problem Formulation

To ensure that the signal power can still reach the target efficiently under MRR process variation, the probability distribution of the signal transmission efficiency at the ports of the MRR must be considered in the design phase.

Due to the unavailability of publicly shared MRR production data at present, I hypothesize, based on the central limit theorem, that the radius of a single MRR follows a normal distribution in large-scale production. The normal distribution can be expressed by the following example based on the content in (Bryc 1995):

Example 3.3. The probability density function (PDF) $f_X(x)$ of a **normal distribution** X with mean μ and standard deviation σ, denoted as $X \sim \mathcal{N}(\mu, \sigma^2)$, is given by:

$$f_X(x) = \frac{1}{\sigma\sqrt{2\pi}} e^{-\frac{(x-\mu)^2}{2\sigma^2}}.$$

The density function $f_Z(x)$ of a **standard normal distribution** $Z = \frac{X-\mu}{\sigma}$ is given by taking $\mu = 0$ and $\sigma^2 = 1$:

$$f_Z(x) = \frac{1}{\sqrt{2\pi}} e^{-\frac{x^2}{2}}.$$

The cumulative distribution function (CDF) of the standard normal distribution, denoted by

Φ, is given by the integral:

$$\Phi(x) = P(Z \leq x) = \int_{-\infty}^{x} \frac{1}{\sqrt{2\pi}} e^{-\frac{t^2}{2}}\, dt.$$

The CDF of X can be written as

$$F_X(x) = P(X \leq x) = P(\sigma Z + \mu \leq x) = P(Z \leq \frac{x-\mu}{\sigma}) = \Phi\left(\frac{x-\mu}{\sigma}\right).$$

The central limit theorem is expressed as follows:

Theorem 3.4 (Central limit theorem (CLT) (Klenke 2006))**.** *For $n \in \mathbb{N}$, let $X_1, X_2, \ldots, X_n$ be a sequence of independent and identically distributed random variables with mean $\mu := \mathbb{E}[X_1]$, variance $\sigma^2 := Var[X_1] \in [0, \infty)$ and $S_n^* := \frac{1}{\sqrt{n}} \sum_{i=1}^{n} \frac{(X_i - \mu)}{\sigma}$. As $n \to \infty$, the distribution of S_n^* converges weakly to the standard normal distribution $N(0, 1)$. Then*

$$\lim_{n\to\infty} P(S_n^* \in [a, b]) = \frac{1}{\sqrt{2\pi}} \int_a^b e^{-\frac{x^2}{2}}\, dx$$

for $-\infty \leq a < b \leq +\infty$.

Proof. The proof can be found on page 321 of book (Klenke 2006). □

In large-scale production processes, the MRR radius can be affected by numerous independent random factors, including lithography and etching processes, material consistency, equipment accuracy, environmental conditions, and others. These factors are considered independent random variables, each of which can cause small changes in the MRR radius. According to Theorem 3.4, if the effects of a large number of independent random variables are relatively small, then the sum or average of these variables will be approximately normally distributed, regardless of the distribution of these independent variables themselves. It is reasonable to assume that in large-scale production, the MRR radius affected by numerous independent random factors follows a normal distribution. Then, the radius can be written as a random variable $R \sim N(r, \sigma^2)$. In this case, $r \in \mathbb{R}^+$ represents the nominal radius without process variation of the designed MRR, and σ describes the standard deviation introduced during the process variation.

Considering that the radius of the MRR follows a normal distribution, signals of different wavelengths and MRRs of different radii exhibit their own transmission efficiency probability distribution at each port. To accurately quantify the effect of process variation on the power transmission capability of signals at each MRR port, I adopt the expected value as a statistical measure. This concept is detailed in the following definition:

Definition 3.5. (Durrett 2019) Let X be a real-valued integrable and random variable on $(\Omega, \mathcal{F}, P)$. If X is a discrete random variable with probability mass function $p_X(x)$, then the **expected value** of X is defined as:

$$\mathbb{E}[X] = \sum_{x \in \Omega} x \cdot p_X(x).$$

If X is a continuous random variable with probability density function $f_X(x)$, then the **expected value** of X is defined as:

$$\mathbb{E}[X] = \int_{\Omega} X \, dP = \int_{\Omega} x \cdot f_X(x) \, dx.$$

The expected value essentially provides a "mean" outcome for the random variable X, taking into account the various possibilities of its outcomes and their associated probabilities. The expected value of power transmission efficiency serves as a metric that aggregates the power transmission efficiencies at various possible MRR radii weighted by their respective probabilities in the radius normal distribution. For brevity, this term will be referred to as **"expected transmission efficiency"** in the following sections.

The random variable R follows a normal distribution with mean r and variance σ^2, denoted by $R \sim N(r, \sigma^2)$. The expected transmission efficiency of the signal on wavelength λ_l at the drop port of the MRR with radius R can be then expressed as $\mathbb{E}[H_{\text{drop}}(R, \lambda_l)]$. Similarly, the expected transmission efficiency of the signal on wavelength λ_l at the through port of the MRR with radius R can be denoted as $\mathbb{E}[H_{\text{through}}(R, \lambda_l)]$. Now, a model of the expected transmission efficiency of a signal sent by the master and received by the slave can be constructed. The formulation of this model relies on the introduction of several additional parameters that extend the basic parameters presented in Section 3.1:

$\mathcal{R}$: The set of available radius options, with $|\mathcal{R}|$ denoting the total number of radius options.

r_x**:** The x-th radius among these options, where $x \in |\mathcal{R}|$.

Λ**:** The set of available wavelength options, with $|\Lambda|$ denoting the total number of wavelength options.

λ_l**:** The l-th wavelength in the options, where $l \in |\Lambda|$.

σ**:** The standard deviation representing the variation during the fabrication process.

Consequently, a model of the expected transmission efficiency of the signal sent by the master and received by the slave can be formalized as follows:

Definition 3.6. It is assumed that all MRRs in the network topology are subject to the same process variation error. The expected transmission efficiency of signal (m_i, s_j), denoted by $\mathbb{E}[H_{(m_i,s_j)}]$, is given as

$$\mathbb{E}[H_{(m_i,s_j)}] = (1-cl)^{c_{(m_i,s_j)}} \prod_{mrr_h \in \mathcal{MRR}^{\text{drop}}_{(m_i,s_j)}} \mathbb{E}[H_{\text{drop}}(R_x, \lambda_l)] \prod_{mrr_f \in \mathcal{MRR}^{\text{through}}_{(m_i,s_j)}} \mathbb{E}[H_{\text{through}}(R_y, \lambda_l)]. \tag{3.9}$$

Here, λ_l is the signal wavelength. R_x and R_y are independent random variables following the normal distribution, with $R_x \sim N(r_x, \sigma^2)$ and $R_y \sim N(r_y, \sigma^2)$. The parameters r_x and r_y denote the nominal radii of mrr_h and mrr_f, while σ represents the standard deviation due to the process variation error.

Transmission efficiency is often expressed in decibels (dB), which are used to compare the intensity of two signals or a change in the power level of a signal. In addition, when powers are multiplied together, the corresponding decibel values can be added directly.

Definition 3.7. The input power S_{input} is set to 1 Watt as 1 unit. Let $\mathbb{E}[H_{\text{drop}}(R_x, \lambda_l)]_{\text{dB}}$ and $\mathbb{E}[H_{\text{through}}(R_x, \lambda_l)]_{\text{dB}}$ represent the expected transmission efficiencies of a signal on wavelength λ_l at the drop port and the through port of an MRR with radius R_x, respectively, all expressed in dB. These expected transmission efficiencies can be converted using the following expressions:

$$\begin{aligned} \mathbb{E}[H_{\text{drop}}(R_x, \lambda_l)]_{\text{dB}} &= 10 \log_{10} \left(\frac{\mathbb{E}[H_{\text{drop}}(R_x, \lambda_l)]}{S_{\text{input}}} \right) \\ &= 10 \log_{10} \mathbb{E}[H_{\text{drop}}(R_x, \lambda_l)]; \end{aligned} \tag{3.10}$$

$$\mathbb{E}[H_{\text{through}}(R_x, \lambda_l)]_{dB} = 10\log_{10}\left(\frac{\mathbb{E}[H_{\text{through}}(R_x, \lambda_l)]}{S_{\text{input}}}\right)$$
$$= 10\log_{10}\mathbb{E}[H_{\text{through}}(R_x, \lambda_l)]. \tag{3.11}$$

Conversely,

$$\mathbb{E}[H_{\text{drop}}(R_x, \lambda_l)] = 10^{\frac{\mathbb{E}[H_{\text{drop}}(R_x, \lambda_l)]_{\text{dB}}}{10}}, \tag{3.12}$$

and

$$\mathbb{E}[H_{\text{through}}(R_x, \lambda_l)] = 10^{\frac{\mathbb{E}[H_{\text{through}}(R_x, \lambda_l)]_{\text{dB}}}{10}}. \tag{3.13}$$

Here, R_x follows the normal distribution, with $R_x \sim N(r_x, \sigma^2)$. The parameter r_x denotes the nominal radius, while σ represents the standard deviation due to the process variation error.

$\mathbb{E}[H_{(m_i,s_j)}]_{\text{dB}}$ represents the expected transmission efficiency of signal (m_i, s_j) in dB, which can be calculated as:

$$\mathbb{E}[H_{(m_i,s_j)}]_{dB} = 10\log_{10}\left(\frac{\mathbb{E}[H_{(m_i,s_j)}]}{S_{\text{input}}}\right)$$
$$= 10\log_{10}\mathbb{E}[H_{(m_i,s_j)}]. \tag{3.14}$$

The transmission efficiency after a wavegudie crossing, expressed in dB, can be defined as follows:

$$(1-cl)_{dB} = 10\log_{10}\left(\frac{1-cl}{S_{\text{input}}}\right)$$
$$= 10\log_{10}(1-cl). \tag{3.15}$$

Conversely,

$$1 - cl = 10^{\frac{(1-cl)_{dB}}{10}}. \tag{3.16}$$

Theorem 3.8. *The expected transmission efficiency of signal (m_i, s_j) in unit dB, denoted as*

$\mathbb{E}[H_{(m_i,s_j)}]_{dB}$, *can be calculated as follows:*

$$\mathbb{E}[H_{(m_i,s_j)}]_{dB} = c_{(m_i,s_j)} \cdot (1-cl)_{dB} + \sum_{mrr_h \in \mathcal{MRR}^{drop}_{(m_i,s_j)}} \mathbb{E}[H_{drop}(R_x,\lambda_l)]_{dB} + \sum_{mrr_f \in \mathcal{MRR}^{through}_{(m_i,s_j)}} \mathbb{E}[H_{through}(R_y,\lambda_l)]_{dB}. \tag{3.17}$$

Here, R_x *and* R_y *are considered as independent random variables, each following a normal distribution, where* $R_x \sim N(r_x,\sigma^2)$ *and* $R_y \sim N(r_y,\sigma^2)$*. The parameters* r_x *and* r_y *denote the nominal radii of* mrr_h *and* mrr_f *in the transmission path of signal* (m_i,s_j)*, respectively, while* σ *stands for the standard deviation due to the process variation error. Additionally,* λ_l *represents the wavelength of signal* (m_i,s_j)*.*

Proof. Using Definition 3.7, $\mathbb{E}[H_{(m_i,s_j)}]_{\mathrm{dB}}$ can be converted as

$$\mathbb{E}[H_{(m_i,s_j)}]_{\mathrm{dB}} = 10\log_{10}\mathbb{E}[H_{(m_i,s_j)}]. \tag{3.18}$$

Then, applying Definition 3.6:

$$\mathbb{E}[H_{(m_i,s_j)}]_{\mathrm{dB}} = 10\log_{10}\mathbb{E}[H_{(m_i,s_j)}]$$

$$= 10\log_{10}\left((1-cl)^{c_{(m_i,s_j)}} \prod_{mrr_h \in \mathcal{MRR}^{\mathrm{drop}}_{(m_i,s_j)}} \mathbb{E}[H_{\mathrm{drop}}(R_x,\lambda_l)] \prod_{mrr_f \in \mathcal{MRR}^{\mathrm{through}}_{(m_i,s_j)}} \mathbb{E}[H_{\mathrm{through}}(R_y,\lambda_l)]\right)$$

$$= 10\log_{10}\left((10^{\frac{(1-cl)_{\mathrm{dB}}}{10}})^{c_{(m_i,s_j)}} \prod_{mrr_h \in \mathcal{MRR}^{\mathrm{drop}}_{(m_i,s_j)}} 10^{\frac{\mathbb{E}[H_{\mathrm{drop}}(R_x,\lambda_l)]_{\mathrm{dB}}}{10}} \prod_{mrr_f \in \mathcal{MRR}^{\mathrm{through}}_{(m_i,s_j)}} 10^{\frac{\mathbb{E}[H_{\mathrm{through}}(R_y,\lambda_l)]_{\mathrm{dB}}}{10}}\right)$$

$$= 10\log\left((10^{\frac{(1-cl)_{\mathrm{dB}}}{10}})^{c_{(m_i,s_j)}} 10^{\frac{\sum_{mrr_h \in \mathcal{MRR}^{\mathrm{drop}}_{(m_i,s_j)}} \mathbb{E}[H_{\mathrm{drop}}(R_x,\lambda_l)]_{\mathrm{dB}}}{10}} 10^{\frac{\sum_{mrr_f \in \mathcal{MRR}^{\mathrm{through}}_{(m_i,s_j)}} \mathbb{E}[H_{\mathrm{though}}(R_y,\lambda_l)]_{\mathrm{dB}}}{10}}\right)$$

$$= 10\log\left((10^{\frac{(1-cl)_{\mathrm{dB}}}{10}})^{c_{(m_i,s_j)}} 10^{\frac{\sum_{mrr_h \in \mathcal{MRR}^{\mathrm{drop}}_{(m_i,s_j)}} \mathbb{E}[H_{\mathrm{drop}}(R_x,\lambda_l)]_{\mathrm{dB}} + \sum_{mrr_f \in \mathcal{MRR}^{\mathrm{through}}_{(m_i,s_j)}} \mathbb{E}[H_{\mathrm{though}}(R_y,\lambda_l)]_{\mathrm{dB}}}{10}}\right)$$

$$= c_{(m_i,s_j)}(1-cl)_{\text{dB}} + \sum_{mrr_h \in \mathcal{MRR}^{\text{drop}}_{(m_i,s_j)}} \mathbb{E}[H_{\text{drop}}(R_x,\lambda_l)]_{\text{dB}} + \sum_{mrr_f \in \mathcal{MRR}^{\text{through}}_{(m_i,s_j)}} \mathbb{E}[H_{\text{though}}(R_y,\lambda_l)]_{\text{dB}}. \tag{3.19}$$

□

In WRONoC, the worst-case transmission efficiency among all signals is a critical factor because it determines the laser power required while ensuring the desired performance. Given the context of process variation, it is essential to calculate the expected transmission efficiency of each signal and identify the worst-case expected transmission efficiency of all signals to determine the required expected compensating power. Therefore, $\mathbb{E}[H_{\text{worst}}]$ is defined as the worst expected transmission efficiency of all signals, and its decibel value is represented as $\mathbb{E}[H_{\text{worst}}]_{\text{dB}}$.

Definition 3.9. Let $\mathbb{E}[H_{\text{worst}}]_{\text{dB}}$ represent the worst-case expected transmission efficiency among all signals in dB. If the input power S_{input} is set to 1 Watt as 1 unit, then

$$\begin{aligned}\mathbb{E}[H_{\text{worst}}]_{\text{dB}} &= 10\log_{10}\left(\frac{\mathbb{E}[H_{\text{worst}}]}{S_{\text{input}}}\right)\\ &= 10\log_{10}\mathbb{E}[H_{\text{worst}}].\end{aligned} \tag{3.20}$$

Consequently, the goal of this work is to maximize the value of $\mathbb{E}[H_{\text{worst}}]_{\text{dB}}$ in the presence of process variation, which is accomplished by optimizing both the selection of MRR radii and signal wavelengths.

3.4.1. Inputs

The following inputs are necessary for the problem formulation:

- A topology of the WRONoC. This should specify the master and slave nodes for each signal, the set of MRRs for different routing requirements (i.e., drop MRR or through MRR) of the signal, and the number of waveguide crossings in the transmission path of the signal.

- A set of options for MRR radii.
- A set of wavelength options for data transmission.
- The standard deviation resulting from the process variation.
- The coefficient accounting for the crossing loss.

3.4.2. Outputs

The solutions, serving as the outputs of the optimization problem, yield:

- The selected radius for each MRR within the topology.
- The specific wavelength value of each signal.

3.4.3. Objective

The primary objective of the problem is to maximize $\mathbb{E}[H_{\text{worst}}]_{\text{dB}}$, which is the worst expected transmission efficiency in dB among all signals.

4. Analytical Stochastic Modeling and Analysis of Expected Transmission Efficiency

Before optimizing the expected transmission efficiency of all signals under process variation, it is critical to first determine the signal expected transmission efficiency at the drop and through ports of an individual MRR based on the input settings. This chapter begins with a review of the fundamentals of probability theory. These principles are then used to model the expected transmission efficiency of an MRR, taking into account process variation. Once the model development is completed, an analysis is performed. The derived expected transmission efficiency then becomes the input for the upcoming optimization process.

4.1. Probability Theory

In this section, I provide the probability theoretical foundation for the mathematical model to be introduced shortly. This section is primarily based on the content presented in (Durrett 2019). The definitions, theorems, and examples discussed in this section are derived from this source unless otherwise indicated.

Let Ω be a non-empty set, and let $\mathcal{F}$ be a subset of 2^{Ω}. In this context, the term **countable** is interpreted to mean either **finite** or **countably infinite**. The set Ω represents the space of elementary events, while $\mathcal{F}$ represents a collection of events.

Definition 4.1. A collection of sets $\mathcal{F}$ is called a ***σ*-algebra** if it satisfies the following three conditions:

(i) $\Omega \in \mathcal{F}$.

(ii) If $A \in \mathcal{F}$, then $A^c \in \mathcal{F}$, and

(iii) If $A_i \in \mathcal{F}$ is a countable sequence of sets, then $\bigcup_i A_i \in \mathcal{F}$.

Definition 4.2. A pair $(\Omega, \mathcal{F})$ is called a **measurable space**.

Definition 4.3. A **measure** μ on a measurable space $(\Omega, \mathcal{F})$ is a non-negative countably additive set function that satisfies:

(i) $\mu(\emptyset) = 0$,

(ii) $\mu(A) \geq 0$ for all $A \in \mathcal{F}$, and

(iii) for a countable sequence of disjoint sets $A_i \in \mathcal{F}$, it holds that $\mu(\bigcup_i A_i) = \sum_i \mu(A_i)$.

μ is called a **probability measure** if μ is a **measure** and $\mu(\Omega) = 1$. In this work, the probability measure is denoted as P.

Definition 4.4. Let (Ω, τ) be a topological space. The σ-algebra $\mathcal{B}(\Omega) := \mathcal{B}(\Omega, \tau) := \sigma(\tau)$, generated by the open sets, is referred to as the **Borel $\boldsymbol{\sigma}$-algebra** on Ω. The elements $A \in \mathcal{B}(\Omega, \tau)$ are called the **Borel sets** of (Ω, τ).

Definition 4.5. A function $X : \Omega \mapsto \mathbb{R}$ is called a **random variable** if, for every Borel set $B \subset \mathbb{R}$, it holds that $X^{-1}(B) = \{\omega : X(\omega) \in B\} \in \mathcal{F}$.

Definition 4.6. For a discrete random variable X on a sample space Ω, the **probability mass function (PMF)** $p_X(x) : \mathbb{R} \to [0, 1]$ of X is defined by $p_X(x) = P(X = x)$. The PMF satisfies the following conditions:

(i) $p_X(x) \geq 0$ for all $x \in \Omega$,

(ii) $\sum_{x \in \Omega} p_X(x) = 1$.

For a continuous random variable X on a sample space Ω, the **probability density function (PDF)** is a function $f_X(x)$ that satisfies the following conditions:

(i) $f_X(x) \geq 0$ for all $x \in \Omega$,

(ii) $\int_\Omega f_X(x)dx = 1$.

Definition 4.7. The **variance** of a random variable X, denoted by $\mathrm{Var}(X)$, is defined as

$$\mathrm{Var}(X) = \mathbb{E}[(X - \mathbb{E}[X])^2].$$

Definition 4.8. (i) σ-fields $\mathcal{F}_1, \mathcal{F}_2, \ldots, \mathcal{F}_n$ are **independent** if for any $A_i \in \mathcal{F}_i$ with $i = 1, \ldots, n$, the following holds:

$$P\left(\bigcap_{i=1}^{n} A_i\right) = \prod_{i=1}^{n} P(A_i).$$

(ii) Random variables $X_1, \ldots, X_n$ are **independent** if for any Borel sets $B_i \in \mathbb{R}$ with $i = 1, \ldots, n$, the following holds:

$$P\left(\bigcap_{i=1}^{n} \{X_i \in B_i\}\right) = \prod_{i=1}^{n} P(X_i \in B_i).$$

(iii) Sets $A_1, \ldots, A_n$ are **independent** if for any subset $I \subset \{1, \ldots, n\}$, the following holds:

$$P\left(\bigcap_{i \in I} A_i\right) = \prod_{i \in I} P(A_i).$$

Theorem 4.9. *Let $X_1, \ldots, X_n$ be independent random variables. If either*

(a) $X_i \geq 0$ for all $i = 1, \ldots, n$, or

(b) $\mathbb{E}[|X_i|] < \infty$ for all $i = 1, \ldots, n$, then

$$\mathbb{E}\left[\prod_{i=1}^{n} X_i\right] = \prod_{i=1}^{n} \mathbb{E}[X_i].$$

Proof. The proof can be found on page 49 of book (Durrett 2019). □

Definition 4.10. A sequence of random variables Y_n converges to a random variable Y *in probability* if for every $\epsilon > 0$, $\lim_{n\to\infty} \mathbb{P}(|Y_n - Y| > \epsilon) = 0$.

Theorem 4.11 (Weak Law of Large Numbers)**.** *Let $X_1, X_2, \ldots$ be a sequence of independent and identically distributed random variables satisfying $\lim_{x\to\infty} x\mathbb{P}(|X_i| > x) = 0$. Define $S_n = \sum_{i=1}^{n} X_i$ and $\mu_n = \mathbb{E}[X_1 1_{\{|X_1| \leq n\}}]$. Then as $n \to \infty$, $(S_n/n - \mu_n)$ converges to 0 in probability.*

Proof. The proof can be found on page number 63 in the book (Durrett 2019). □

4.2. Derivation of the Analytical Stochastic Model

This section presents the derivation of the signal expected transmission efficiency at the drop and through ports of an MRR. The derivation uses the cumulative distribution function (CDF), which is defined as follows:

Definition 4.12. (Durrett 2019) Let X be a random variable.

(i) The probability measure $P_X := P \circ X^{-1}$ is referred to as the **distribution** of X.

(ii) If X is a real random variable, the function $F_X(x) = P(X \leq x) = \int_{-\infty}^{x} f_X(y)dy$ is known as the **cumulative distribution function** of X.

Let the radius be a random variable $R \sim N(r, \sigma^2)$. In this case, $r \in \mathbb{R}^+$ represents the nominal radius of the designed MRR, and σ describes the standard deviation introduced during the fabrication process variation. I start by specifying the range of transmission efficiency without process variation.

Lemma 4.13. *The transmission efficiency of the signal on wavelength λ at the drop port of the MRR with radius r, denoted by $H_{drop}(r, \lambda) = \frac{k^2 k^2}{1-2t^2 cos(\phi)+(t^2)^2}$, where $k, t \in [0, 1]$ and $r, \lambda \in \mathbb{R}^+$, satisfies the following inequality:*

$$\frac{k^4}{(2-k^2)^2} \leq H_{drop}(r, \lambda) \leq 1. \tag{4.1}$$

Proof. Since $\cos(\phi) \in [-1, 1]$, it follows that

$$-2t^2 \cos(\phi) \in [-2t^2, 2t^2] \implies 1 - 2t^2 \cos(\phi) + t^4 \in [1 + t^4 - 2t^2, 1 + t^4 + 2t^2].$$

It can be observed that

$$\frac{k^4}{1 - 2t^2 \cos(\phi) + t^4} \in \left[\frac{k^4}{1 + t^4 + 2t^2}, \frac{k^4}{1 + t^4 - 2t^2}\right].$$

Given the condition $k^2+t^2=1$, noting that $1+t^4+2t^2=(1+t^2)^2=(1+1-k^2)^2=(2-k^2)^2\geq 1$ for $k\in[0,1]$ and $1+t^4-2t^2=(1-t^2)^2=(k^2)^2=k^4$, the inequality can be rewritten as:

$$\frac{k^4}{1-2t^2\cos(\phi)+t^4}\in\left[\frac{k^4}{(2-k^2)^2},\frac{k^4}{k^4}\right]\implies\frac{k^4}{1-2t^2\cos(\phi)+t^4}\in\left[\frac{k^4}{(2-k^2)^2},1\right].$$

This establishes the range of $H_{\text{drop}}(r,\lambda)$. □

Lemma 4.14. *The transmission efficiency of the signal on wavelength λ at the through port of the MRR with radius r, denoted by $H_{through}(r,\lambda)=1-H_{drop}(r,\lambda)=1-\frac{k^2k^2}{1-2t^2cos(\phi)+(t^2)^2}$, where $k,t\in[0,1]$ and $r,\lambda\in\mathbb{R}^+$, satisfies the following inequality:*

$$0\leq H_{through}(r,\lambda)\leq 1-\frac{k^4}{(2-k^2)^2}. \tag{4.2}$$

Proof. Recall from Lemma 4.13 that the range of $H_{\text{drop}}(r,\lambda)$ is given by $[\frac{k^4}{(2-k^2)^2},1]$, it follows that $-H_{\text{drop}}(r,\lambda)\in[-1,-\frac{k^4}{(2-k^2)^2}]$. Since $H_{\text{through}}(r,\lambda)=1-H_{\text{drop}}(r,\lambda)$, it yields that $H_{\text{through}}(r,\lambda)\in[1-1,1-\frac{k^4}{(2-k^2)^2}]\implies H_{\text{through}}(r,\lambda)\in[0,1-\frac{k^4}{(2-k^2)^2}]$. □

The next step is to derivate its cumulative distributions:

Theorem 4.15. *The cumulative distribution function of $H_{drop}(R,\lambda)$ for $R\sim N(r,\sigma^2)$ is*

$$\sum_{n\in\mathbb{Z}}\left[\Phi\left(\frac{\frac{2\pi(n+1)-\arccos\left(\frac{1-\frac{k^4}{y}+(t^2)^2}{2t^2}\right)}{2\pi\beta(\lambda)}-r}{\sigma}\right)-\Phi\left(\frac{\frac{2n\pi+\arccos\left(\frac{1-\frac{k^4}{y}+(t^2)^2}{2t^2}\right)}{2\pi\beta(\lambda)}-r}{\sigma}\right)\right], \tag{4.3}$$

where $r,\lambda\in\mathbb{R}^+$ and $\sigma\geq 0$.

Proof. Using Example 3.3, the density function of the random variable radius R can be written as:

$$f_R(x)=\frac{1}{\sigma\sqrt{2\pi}}e^{-\frac{(x-r)^2}{2\sigma^2}}. \tag{4.4}$$

The cumulative distribution function of R is given by:

$$F_R(x) = \Phi(\frac{x-r}{\sigma}). \tag{4.5}$$

Let $Y = H_{\text{drop}}(R, \lambda)$ be a random variable. The cumulative distribution function of Y is denoted by $G_Y(y)$ and defined by Definition 4.12. By Lemma 4.13, $y \in [\frac{k^4}{(2-k^2)^2}, 1]$. Then

$$G_Y(y) = P(Y \leq y) = P(H_{\text{drop}}(R, \lambda) \leq y). \tag{4.6}$$

Applying Equation (3.5) of $H_{\text{drop}}(r, \lambda)$, the distribution function can be calculated as:

$$\begin{aligned}
G_Y(y) &= P(Y \leq y) \\
&= P(H_{\text{drop}}(R, \lambda) \leq y) \\
&= P\left(\frac{k^2 k^2}{1 - 2t^2\cos(\phi(R, \lambda)) + (t^2)^2} \leq y\right) \\
&\overset{(3.3)}{=} P\left(\frac{k^4}{1 - 2t^2\cos(2\pi R\beta(\lambda)) + (t^2)^2} \leq y\right) \\
&= P\left(1 - 2t^2\cos(2\pi R\beta(\lambda)) + (t^2)^2 \geq \frac{k^4}{y}\right) \\
&= P\left(-2t^2\cos(2\pi R\beta(\lambda)) \geq \frac{k^4}{y} - 1 - (t^2)^2\right) \\
&= P\left(2t^2\cos(2\pi R\beta(\lambda)) \leq -\frac{k^4}{y} + 1 + (t^2)^2\right) \\
&= P\left(\cos(2\pi R\beta(\lambda)) \leq \frac{1 - \frac{k^4}{y} + (t^2)^2}{2t^2}\right).
\end{aligned} \tag{4.7}$$

The range of y can be employed to investigate whether the range of

$$\frac{1 - \frac{k^4}{y} + (t^2)^2}{2t^2}$$

satisfying the domain of arccos function, which is $[-1, 1]$:

$$y \geq \frac{k^4}{(2-k^2)^2} \overset{k^2+t^2=1}{\Longrightarrow} y \geq \frac{k^4}{(1+t^2)^2}$$

$$
\begin{aligned}
&\implies \frac{k^4}{y} \leq (1+t^2)^2 \\
&\implies \frac{k^4}{y} \leq 2t^2 + 1 + t^4 \\
&\implies \frac{k^4}{y} - 1 - t^4 \leq 2t^2 \\
&\implies \frac{\frac{k^4}{y} - 1 - (t^2)^2}{2t^2} \leq 1 \\
&\implies \frac{1 - \frac{k^4}{y} + (t^2)^2}{2t^2} \geq -1,
\end{aligned} \tag{4.8}
$$

and

$$
\begin{aligned}
y \leq 1 &\implies y \leq \frac{k^4}{k^4} \\
&\overset{k^2+t^2=1}{\implies} y \leq \frac{k^4}{(1-t^2)^2} \\
&\implies \frac{k^4}{y} \geq 1 + t^4 - 2t^2 \\
&\implies -\frac{k^4}{y} \leq -1 - t^4 + 2t^2 \\
&\implies -\frac{k^4}{y} + 1 + t^4 \leq 2t^2 \\
&\implies \frac{1 - \frac{k^4}{y} + t^4}{2t^2} \leq 1.
\end{aligned} \tag{4.9}
$$

Since both conditions hold, it can be concluded that the range of $\frac{1-\frac{k^4}{y}+(t^2)^2}{2t^2}$ satisfies the domain of the arccos function. Then

$$
G_Y(y) = \sum_{n\in\mathbb{Z}} P\left(2n\pi + \arccos\left(\frac{1-\frac{k^4}{y}+(t^2)^2}{2t^2}\right) \leq 2\pi R\beta(\lambda) \leq 2\pi(n+1) - \arccos\left(\frac{1-\frac{k^4}{y}+(t^2)^2}{2t^2}\right)\right)
$$

$$
\begin{aligned}
&\overset{2\pi\beta(\lambda)>0}{=} \sum_{n\in\mathbb{Z}} P\left(\frac{2n\pi + \arccos\left(\frac{1-\frac{k^4}{y}+(t^2)^2}{2t^2}\right)}{2\pi\beta(\lambda)} \leq R \leq \frac{2\pi(n+1) - \arccos\left(\frac{1-\frac{k^4}{y}+(t^2)^2}{2t^2}\right)}{2\pi\beta(\lambda)}\right) \\
&= \sum_{n\in\mathbb{Z}} \left[P\left(R \leq \frac{2\pi(n+1) - \arccos\left(\frac{1-\frac{k^4}{y}+(t^2)^2}{2t^2}\right)}{2\pi\beta(\lambda)}\right) - P\left(R \leq \frac{2n\pi + \arccos\left(\frac{1-\frac{k^4}{y}+(t^2)^2}{2t^2}\right)}{2\pi\beta(\lambda)}\right)\right] \\
&= \sum_{n\in\mathbb{Z}} \left[F_R\left(\frac{2\pi(n+1) - \arccos\left(\frac{1-\frac{k^4}{y}+(t^2)^2}{2t^2}\right)}{2\pi\beta(\lambda)}\right) - F_R\left(\frac{2n\pi + \arccos\left(\frac{1-\frac{k^4}{y}+(t^2)^2}{2t^2}\right)}{2\pi\beta(\lambda)}\right)\right] \\
&= \sum_{n\in\mathbb{Z}} \left[\Phi\left(\frac{\frac{2\pi(n+1) - \arccos\left(\frac{1-\frac{k^4}{y}+(t^2)^2}{2t^2}\right)}{2\pi\beta(\lambda)} - r}{\sigma}\right) - \Phi\left(\frac{\frac{2n\pi + \arccos\left(\frac{1-\frac{k^4}{y}+(t^2)^2}{2t^2}\right)}{2\pi\beta(\lambda)} - r}{\sigma}\right)\right].
\end{aligned}
\tag{4.10}
$$

□

Theorem 4.16. *The cumulative distribution function of $H_{through}(R,\lambda)$ for $R \sim N(r,\sigma^2)$ is*

$$
\sum_{n\in\mathbb{Z}} \left[\Phi\left(\frac{\frac{2\pi n + \arccos\left(\frac{1-\frac{k^4}{1-z}+(t^2)^2}{2t^2}\right)}{2\pi\beta(\lambda)} - r}{\sigma}\right) - \Phi\left(\frac{\frac{2n\pi - \arccos\left(\frac{1-\frac{k^4}{1-z}+(t^2)^2}{2t^2}\right)}{2\pi\beta(\lambda)} - r}{\sigma}\right)\right], \tag{4.11}
$$

where $r, \lambda \in \mathbb{R}^+$ and $\sigma \geq 0$.

Proof. Using Example 3.3, the density function of the random variable radius R is defined as

$$
f_R(x) = \frac{1}{\sigma\sqrt{2\pi}} e^{-\frac{(x-r)^2}{2\sigma^2}}. \tag{4.12}
$$

The cumulative distribution function of R is given by

$$F_R(x) = \Phi(\frac{x-r}{\sigma}). \tag{4.13}$$

Let $Z = H_{\text{through}}(R, \lambda)$ be a random variable. The cumulative distribution function of Z is denoted by $G_Z(z)$ and is defined by Definition 4.12. By Lemma 4.14, $z \in [0, 1 - \frac{k^4}{(2-k^2)^2}]$. Then

$$G_Z(z) = P(Z \leq z) = P(H_{\text{though}}(R, \lambda) \leq z).$$

Applying Equation (3.6) of H_{through}, the cumulative distribution function can be calculated as:

$$\begin{aligned}
G_Z(z) &= P(Z \leq z) \\
&= P(H_{\text{through}}(R, \lambda) \leq z) \\
&= P(1 - H_{\text{drop}}(R, \lambda) \leq z) \\
&= P\left(1 - \frac{k^2 k^2}{1 - 2t^2\cos(\phi(R, \lambda)) + (t^2)^2} \leq z\right) \\
&= P\left(-\frac{k^2 k^2}{1 - 2t^2\cos(\phi(R, \lambda)) + (t^2)^2} \leq z - 1\right) \\
&= P\left(\frac{k^2 k^2}{1 - 2t^2\cos(\phi(R, \lambda)) + (t^2)^2} \geq 1 - z\right) \\
&\overset{(3.3)}{=} P\left(\frac{k^4}{1 - 2t^2\cos(2\pi R\beta(\lambda)) + (t^2)^2} \geq 1 - z\right) \\
&= P\left(1 - 2t^2\cos(2\pi R\beta(\lambda)) + (t^2)^2 \leq \frac{k^4}{1-z}\right) \\
&= P\left(-2t^2\cos(2\pi R\beta(\lambda)) \leq \frac{k^4}{1-z} - 1 - (t^2)^2\right) \\
&= P\left(2t^2\cos(2\pi R\beta(\lambda)) \geq -\frac{k^4}{1-z} + 1 + (t^2)^2\right) \\
&= P\left(\cos(2\pi R\beta(\lambda)) \geq \frac{1 - \frac{k^4}{1-z} + (t^2)^2}{2t^2}\right).
\end{aligned} \tag{4.14}$$

The range of z can be used to investigate whether the range of

$$\frac{1-\frac{k^4}{1-z}+(t^2)^2}{2t^2} \tag{4.15}$$

satisfying the domain of arccos function, which is $[-1,1]$:

$$\begin{aligned}
z \geq 0 &\implies z \geq 1-\frac{k^4}{k^4} \\
&\implies z \geq 1-\frac{k^4}{(1-t^2)^2} \\
&\implies -z \leq \frac{k^4}{(1-t^2)^2}-1 \\
&\implies 1-z \leq \frac{k^4}{(1-t^2)^2} \\
&\implies 2t^2(1-z) \leq 2t^2\frac{k^4}{(1-t^2)^2} \\
&\implies \frac{k^4}{2t^2(1-z)} \geq \frac{(1-t^2)^2}{2t^2} \\
&\implies \frac{k^4}{2t^2(1-z)} \geq \frac{1+t^4}{2t^2}-1 \\
&\implies -\frac{k^4}{2t^2(1-z)} \leq 1-\frac{1+t^4}{2t^2} \\
&\implies \frac{1+t^4}{2t^2}-\frac{k^4}{2t^2(1-z)} \leq 1 \\
&\implies \frac{1-\frac{k^4}{1-z}+(t^2)^2}{2t^2} \leq 1,
\end{aligned} \tag{4.16}$$

and

$$\begin{aligned}
z \leq 1-\frac{k^4}{(2-k^2)^2} &\implies z \leq 1-\frac{k^4}{(1+t^2)^2} \\
&\implies -z \geq \frac{k^4}{(1+t^2)^2}-1
\end{aligned}$$

$$\implies 1 - z \geq \frac{k^4}{(1+t^2)^2}$$

$$\implies \frac{k^4}{1-z} \leq (1+t^2)^2$$

$$\implies \frac{k^4}{(1-z)2t^2} \leq \frac{(1+2t^2+t^4)}{2t^2}$$

$$\implies \frac{k^4}{(1-z)2t^2} \leq \frac{(1+t^4)}{2t^2} + 1$$

$$\implies -\frac{k^4}{(1-z)2t^2} \geq -\frac{(1+t^4)}{2t^2} - 1$$

$$\implies \frac{(1+t^4)}{2t^2} - \frac{k^4}{(1-z)2t^2} \geq -1 \tag{4.17}$$

Since both conditions hold, it can be concluded that the range of $\frac{(1+t^4)}{2t^2} - \frac{k^4}{(1-z)2t^2}$ satisfies the domain of the arccos function. Then

$$G_Z(z) = \sum_{n\in\mathbb{Z}} P\left(2n\pi - \arccos\left(\frac{1-\frac{k^4}{1-z}+(t^2)^2}{2t^2}\right) \leq 2\pi R\beta(\lambda) \leq 2\pi n + \arccos\left(\frac{1-\frac{k^4}{1-z}+(t^2)^2}{2t^2}\right)\right)$$

$$\overset{2\pi\beta(\lambda)>0}{=} \sum_{n\in\mathbb{Z}} P\left(\frac{2n\pi - \arccos\left(\frac{1-\frac{k^4}{1-z}+(t^2)^2}{2t^2}\right)}{2\pi\beta(\lambda)} \leq R \leq \frac{2\pi n + \arccos\left(\frac{1-\frac{k^4}{1-z}+(t^2)^2}{2t^2}\right)}{2\pi\beta(\lambda)}\right)$$

$$= \sum_{n\in\mathbb{Z}} \left[P\left(R \leq \frac{2\pi n + \arccos\left(\frac{1-\frac{k^4}{1-z}+(t^2)^2}{2t^2}\right)}{2\pi\beta(\lambda)}\right) - P\left(R \leq \frac{2n\pi - \arccos\left(\frac{1-\frac{k^4}{1-z}+(t^2)^2}{2t^2}\right)}{2\pi\beta(\lambda)}\right)\right]$$

$$= \sum_{n\in\mathbb{Z}} \left[F_R\left(\frac{2\pi n + \arccos\left(\frac{1-\frac{k^4}{1-z}+(t^2)^2}{2t^2}\right)}{2\pi\beta(\lambda)}\right) - F_R\left(\frac{2n\pi - \arccos\left(\frac{1-\frac{k^4}{1-z}+(t^2)^2}{2t^2}\right)}{2\pi\beta(\lambda)}\right)\right]$$

$$= \sum_{n\in\mathbb{Z}} \left[\Phi\left(\frac{\frac{2\pi n + \arccos\left(\frac{1-\frac{k^4}{1-z}+(t^2)^2}{2t^2}\right)}{2\pi\beta(\lambda)} - r}{\sigma} \right) - \Phi\left(\frac{\frac{2n\pi - \arccos\left(\frac{1-\frac{k^4}{1-z}+(t^2)^2}{2t^2}\right)}{2\pi\beta(\lambda)} - r}{\sigma} \right) \right]. \tag{4.18}$$

□

The following theorem can be used to calculate the expected value using the cumulative distribution function:

Theorem 4.17. *(Saeed 2000) The expected value of a non-negative continuous random variable X with cumulative distribution function F_X and density function f_X can be computed using the following integral formula:*

$$\mathbb{E}(X) = \int_0^\infty (1 - F_X(t))\ dt. \tag{4.19}$$

Proof. According to Definition 3.5 of the expected value, for $X \geq 0$:

$$\begin{aligned} \mathbb{E}[X] &= \int_0^\infty x f_X(x)\, dx \\ &= \int_0^\infty \left(\int_0^x dt \right) f_X(x)\, dx. \end{aligned} \tag{4.20}$$

Then, the order of integration can be changed:

$$\begin{aligned} \mathbb{E}[X] &= \int_0^\infty \left(\int_t^\infty f_X(x)\, dx \right) dt \\ &= \int_0^\infty P\left(X \geq t\right)\ dt \\ &= \int_0^\infty (1 - F_X(t))\ dt. \end{aligned} \tag{4.21}$$

□

Then, the expected transmission efficiencies of the signal at drop and through ports of an MRR

can be derived.

Theorem 4.18. *The expected value of* $H_{drop}(R,\lambda)$ *with* $R \sim N(r,\sigma^2)$, $r \in \mathbb{R}^+$, $\sigma \geq 0$, *and* $\lambda \in \mathbb{R}^+$ *for* $y \in \left[\frac{k^4}{(2-k^2)^2}, 1\right]$ *is*

$$\mathbb{E}[H_{drop}(R,\lambda)] = \int_{\frac{k^4}{(2-k^2)^2}}^{1} \left(1 - \sum_{n\in\mathbb{Z}} \left[\Phi\left(\frac{\frac{2\pi(n+1)-\arccos\left(\frac{1-\frac{k^4}{y}+(t^2)^2}{2t^2}\right)}{2\pi\beta(\lambda)} - r}{\sigma}\right)\right.\right. \\ \left.\left. - \Phi\left(\frac{\frac{2n\pi+\arccos\left(\frac{1-\frac{k^4}{y}+(t^2)^2}{2t^2}\right)}{2\pi\beta(\lambda)} - r}{\sigma}\right)\right]\right) \mathrm{d}y. \tag{4.22}$$

Proof. Lemma 4.13 establishes the domain of the expected value function as $\left[\frac{k^4}{(2-k^2)^2}, 1\right]$. The cumulative distribution function of $H_{\text{drop}}(R,\lambda)$, denoted by $G_Y(y)$ with $Y = H_{\text{drop}}(R,\lambda)$, can be represented using Theorem 4.15:

$$G_Y(y) = \sum_{n\in\mathbb{Z}} \left[\Phi\left(\frac{\frac{2\pi(n+1)-\arccos\left(\frac{1-\frac{k^4}{y}+(t^2)^2}{2t^2}\right)}{2\pi\beta(\lambda)} - r}{\sigma}\right) - \Phi\left(\frac{\frac{2n\pi+\arccos\left(\frac{1-\frac{k^4}{y}+(t^2)^2}{2t^2}\right)}{2\pi\beta(\lambda)} - r}{\sigma}\right)\right]. \tag{4.23}$$

Applying Theorem 4.17, the expected value of $H_{\text{drop}}(R,\lambda)$ is given as

$$\begin{aligned}
\mathbb{E}[H_{\text{drop}}(R,\lambda)] &= \mathbb{E}[Y] \\
&= \int_{\frac{k^4}{(2-k^2)^2}}^{1} (1 - G_Y(y))\ \mathrm{d}y \\
&= \int_{\frac{k^4}{(2-k^2)^2}}^{1} \left(1 - \sum_{n\in\mathbb{Z}} \left[\Phi\left(\frac{\frac{2\pi(n+1)-\arccos\left(\frac{1-\frac{k^4}{y}+(t^2)^2}{2t^2}\right)}{2\pi\beta(\lambda)} - r}{\sigma}\right)\right.\right.
\end{aligned}$$

$$- \Phi \left(\frac{\frac{2n\pi + \arccos\left(\frac{1-\frac{k^4}{y}+(t^2)^2}{2t^2} \right)}{2\pi\beta(\lambda)} - r}{\sigma} \right] \Bigg) \, \mathrm{d}y. \tag{4.24}$$

□

Theorem 4.19. *The expected value of* $H_{through}(R, \lambda)$ *with* $R \sim N(r, \sigma^2)$, $r \in \mathbb{R}^+$, $\sigma \geq 0$, *and* $\lambda \in \mathbb{R}^+$ *for* $z \in [0, 1 - \frac{k^4}{(2-k^2)^2}]$ *is*

$$\begin{aligned} \mathbb{E}[H_{through}(R, \lambda)] = \int_0^{1-\frac{k^4}{(2-k^2)^2}} \Bigg(1 - \sum_{n \in \mathbb{Z}} \Bigg[\Phi \left(\frac{\frac{2\pi n + \arccos\left(\frac{1-\frac{k^4}{1-z}+(t^2)^2}{2t^2} \right)}{2\pi\beta(\lambda)} - r}{\sigma} \right) \\ - \Phi \left(\frac{\frac{2n\pi - \arccos\left(\frac{1-\frac{k^4}{1-z}+(t^2)^2}{2t^2} \right)}{2\pi\beta(\lambda)} - r}{\sigma} \right) \Bigg] \Bigg) \, \mathrm{d}z. \end{aligned} \tag{4.25}$$

Proof. Lemma 4.14 shows the domain of the expected value function as $\left[0, 1 - \frac{k^4}{(2-k^2)^2}\right]$. The cumulative distribution function of $H_{\text{through}}(R, \lambda)$, denoted by $G_Z(z)$ with $Z = H_{\text{through}}(R, \lambda)$, can be represented using Theorem 4.16:

$$G_Z(z) = \sum_{n \in \mathbb{Z}} \left[\Phi \left(\frac{\frac{2\pi n + \arccos\left(\frac{1-\frac{k^4}{1-z}+(t^2)^2}{2t^2} \right)}{2\pi\beta(\lambda)} - r}{\sigma} \right) - \Phi \left(\frac{\frac{2n\pi - \arccos\left(\frac{1-\frac{k^4}{1-z}+(t^2)^2}{2t^2} \right)}{2\pi\beta(\lambda)} - r}{\sigma} \right) \right]. \tag{4.26}$$

Applying Theorem 4.17, the expected value of $H_{\text{through}}(R, \lambda)$ is given as

$$\mathbb{E}[H_{\text{through}}(R, \lambda)] = \mathbb{E}[Z]$$

$$= \int_0^{1-\frac{k^4}{(2-k^2)^2}} (1 - G_Z(z))\, \mathrm{d}z$$

$$= \int_0^{1-\frac{k^4}{(2-k^2)^2}} \left(1 - \sum_{n\in\mathbb{Z}} \left[\Phi\left(\frac{\frac{2\pi n + \arccos\left(\frac{1-\frac{k^4}{1-z}+(t^2)^2}{2t^2}\right)}{2\pi\beta(\lambda)} - r}{\sigma}\right)\right.\right.$$

$$\left.\left. - \Phi\left(\frac{\frac{2n\pi - \arccos\left(\frac{1-\frac{k^4}{1-z}+(t^2)^2}{2t^2}\right)}{2\pi\beta(\lambda)} - r}{\sigma}\right)\right]\right) \mathrm{d}z. \tag{4.27}$$

□

The linearity property of the expected value can be used as a quick approach to calculating the expected value of $H_{\text{through}}(R, \lambda)$. This property can be formally described by the following theorem:

Theorem 4.20. *(Stein 2005) Let X and Y be two random variables, then*

$$\mathbb{E}[X + Y] = \mathbb{E}[X] + \mathbb{E}[Y]. \tag{4.28}$$

Proof. If X and Y are discrete random variables, their joint probability mass function is denoted by $f_{XY}(x_i, y_j)$. By using Definition 3.5, the expected value of their sum can be computed as follows:

$$\begin{aligned}
\mathbb{E}[X + Y] &= \sum_{i\in\mathbb{Z}} \sum_{j\in\mathbb{Z}} (x_i + y_j) f_{XY}(x_i, y_j) \\
&= \sum_{i\in\mathbb{Z}} \sum_{j\in\mathbb{Z}} x_i f_{XY}(x_i, y_j) + \sum_{i\in\mathbb{Z}} \sum_{j\in\mathbb{Z}} y_j f_{XY}(x_i, y_j) \\
&= \mathbb{E}[X] + \mathbb{E}[Y].
\end{aligned}$$

If X and Y are continuous random variables, then their joint probability density function is

denoted by $f_{XY}(x, y)$. By using Definition 3.5, the expected value of their sum is given by:

$$\begin{aligned}\mathbb{E}[X+Y] &= \int_{-\infty}^{+\infty}\int_{-\infty}^{+\infty}(x+y)f_{XY}(x,y)\,dxdy \\ &= \int_{-\infty}^{+\infty}\int_{-\infty}^{+\infty}xf_{XY}(x,y)\,dxdy + \int_{-\infty}^{+\infty}\int_{-\infty}^{+\infty}yf_{XY}(x,y)\,dxdy \\ &= \mathbb{E}[X]+\mathbb{E}[Y].\end{aligned}$$

□

Theorem 4.21. *The expected value of $H_{through}(R,\lambda)$ with $R \sim N(r,\sigma^2)$, $r \in \mathbb{R}^+$, $\sigma \geq 0$, and $\lambda \in \mathbb{R}^+$ for $z \in [0, 1-\frac{k^4}{(2-k^2)^2}]$ is given by*

$$\mathbb{E}[H_{through}(R,\lambda)] = 1 - \mathbb{E}[H_{drop}(R,\lambda)]. \tag{4.29}$$

Proof. From Equation (3.7), it can be observed that $H_{\text{through}}(R,\lambda) + H_{\text{drop}}(R,\lambda) = 1$. Therefore, based on the linearity property of the expected value in Theorem 4.20, the equation can be rewritten as follows:

$$\begin{aligned}\mathbb{E}[H_{\text{through}}(R,\lambda)] + \mathbb{E}[H_{\text{drop}}(R,\lambda)] &= \mathbb{E}[H_{\text{through}}(R,\lambda) + H_{\text{drop}}(R,\lambda)] \\ &= \mathbb{E}[1] \\ &= 1 \end{aligned} \tag{4.30}$$

$$\implies \mathbb{E}[H_{\text{through}}(R,\lambda)] = 1 - \mathbb{E}[H_{\text{drop}}(R,\lambda)].$$

□

4.3. Expected Transmission Spectral Analysis

Numerical integration is the mainstream method for solving integration problems in computer programs. The core idea is to discretize continuous integration problems to obtain an approximate numerical solution. To perform an analysis of the expected transmission spectra, I used the numerical integration technique of the Riemann summation method in the C++ program to approximate the expected values. It can be formally defined as follows:

Definition 4.22. (Philip 2023) Given a function f defined over the interval $[a, b]$ and a partition $a = x_0 < x_1 < \cdots < x_n = b$, the Riemann sum of f over the partition is defined as

$$\sum_{i=1}^{n} f(x_i^*)(x_i - x_{i-1}),$$

where each x_i^* is any chosen point in the interval $[x_{i-1}, x_i]$.

Theorem 4.23. *(Philip 2023) Let f be a function defined on the closed interval $[a, b]$. The limit of the Riemann sums*

$$\int_a^b f(x)\,dx = \lim_{n\to\infty} \sum_{i=1}^{n} f(x_i^*)(x_i - x_{i-1})$$

exists. The limit is unique and is defined as the definite Riemann integral of the function f over $[a, b]$, where $a = x_0 < x_1 < \cdots < x_n = b$.

I divide the domain of the expected values in Theorem 4.18 and Theorem 4.19 into 1000 equal intervals and use the Riemann sum method to accumulate the areas of these intervals to obtain the approximate expected value. The choice of 1000 subintervals strikes a balance between ensuring accuracy and avoiding excessive computational load.

After specifying the definition of Riemann summation and the setting of the parameters, the expected transmission efficiency of the signal on wavelength λ at the drop port of an MRR with radius $R \sim N(r, \sigma^2)$ can be approximated as follows:

$$\mathbb{E}[H_{\text{drop}}(R,\lambda)] \approx \left(\frac{1-\frac{k^4}{(2-k^2)^2}}{1000}\right) \sum_{i=0}^{1000} \left[1 - \sum_{n\in\mathbb{Z}} \left(\Phi\left(\frac{2\pi(n+1) - \arccos\left(\frac{1-\frac{k^4}{y_i}+(t^2)^2}{2t^2}\right)}{2\pi\beta(\lambda)} - r}{\sigma}\right)\right.\right.$$
$$\left.\left. - \Phi\left(\frac{2n\pi + \arccos\left(\frac{1-\frac{k^4}{y_i}+(t^2)^2}{2t^2}\right)}{2\pi\beta(\lambda)} - r}{\sigma}\right)\right)\right], \tag{4.31}$$

where y_i is the left endpoint of the subinterval. And the transmission efficiency of the signal on

wavelength λ at the through port of an MRR with radius $R \sim N(r, \sigma^2)$ can be approximated as follows:

$$\mathbb{E}[H_{\text{through}}(R,\lambda)] \approx \left(\frac{1-\frac{k^4}{(2-k^2)^2}}{1000}\right) \sum_{i=0}^{1000} \left(1 - \sum_{n\in\mathbb{Z}} \left[\Phi\left(\frac{\frac{2\pi n + \arccos\left(\frac{1-\frac{k^4}{1-z_i}+(t^2)^2}{2t^2}\right)}{2\pi\beta} - r}{\sigma}\right)\right.\right. \tag{4.32}$$

$$\left.\left. - \Phi\left(\frac{\frac{2n\pi - \arccos\left(\frac{1-\frac{k^4}{1-z_i}+(t^2)^2}{2t^2}\right)}{2\pi\beta} - r}{\sigma}\right)\right]\right), \tag{4.33}$$

where z_i is the left endpoint of the subinterval.

In the absence of publicly available specific error data, and considering that the existing process technologies mentioned in Section 3.2 can limit the error to less than 1%, I introduce two types of standard deviations to describe the error due to process variation, the absolute standard deviation, and the relative standard deviation. The absolute standard deviation has constant values regardless of the radius of the MRR. On the other hand, the relative standard deviation is proportional to the radius of the MRR. For example, a relative standard deviation of 1% means that the standard deviation is equal to 1% of the radius. Under the absolute standard deviation setting, I set two different standard deviation values of 5 nm and 10 nm; under the relative standard deviation setting, I similarly set two different standard deviation values of 0.05% and 0.1% for each radius option. For comparative analysis, the scenario where no process variation occurs is also considered, that is, $\sigma = 0$. Then, I set the cross-coupling coefficient k to 0.4 (Li, Shen, Yu, Zhang, Chen & Zhang 2020) and used this to determine the self-coupling coefficient t, the value of which is calculated by the equation $t = \sqrt{1-k^2} = \sqrt{0.84}$. To illustrate the properties of MRRs with different radii in the expected transmission spectra under process variation, I consider two MRRs with radii of 10 μm and 27 μm. The larger MRR has more resonant wavelengths than the smaller MRR in the same wavelength range. Based on all the above conditions, the expected transmission spectra at the drop port and through port for these two representative radii are plotted in the wavelength range of 1500 nm – 1525 nm range with 0.1 nm increments, which are presented in Figures 4.1 – 4.5.

Figure 4.1 shows the transmission spectra without process variation. As seen in Figure 4.1 (a), in the transmission spectra at the drop ports of MRRs, there are three peaks for the 10 μm radius of MRR and seven peaks for the 27 μm radius of MRR. These peaks correspond to the troughs at the through port in Figure 4.1 (b) along the wavelength dimension. Figure 4.1 (a) also shows that the resonance peaks become sharper as the radius increases. This suggests that a larger radius can more effectively limit the passage of non-resonant wavelength signals through the drop port, thus providing more selective transmission.

Figures 4.2 (a) – 4.5 (a) show the expected transmission spectra at the drop port under different types of standard deviations. It is worth noting that as the standard deviation changes, the wavelength corresponding to each peak does not change. As the standard deviation increases, the resonance peaks become broader, indicating that larger process variation make MRRs less effective at restricting the passage through the drop port of non-resonant wavelengths.

In particular, Figure 4.2 (a) and Figure 4.3 (a) show the expected transmission spectra at the drop port of MRRs with different radii under absolute standard deviations. As the absolute standard deviation increases, the peaks of the expected transmission efficiency continue to decrease. However, for the troughs and their adjacent areas, the increase in absolute standard deviation does not induce significant changes. This indicates that the process variation has a significantly larger effect on the resonant wavelengths of the MRR and their neighborhoods than on the non-resonant wavelengths. Under the same absolute standard deviation, the degrees of peak value reduction of MRRs with different radii are generally consistent. Hence, the effect of absolute process variation on the transmission efficiency at the drop port of MRRs with different radii does not show a significant discrepancy.

Instead, for MRRs of different radii, the relative standard deviation condition has a different effect on the expected transmission efficiency. As shown in Figure 4.4 (a) and Figure 4.5 (a), as the relative standard deviation increases, the rate and magnitude of peak reduction at the drop port of MRRs with larger radii exceed those with smaller radii. This is because the relative standard deviation associated with larger radii increases accordingly. Although MRRs with larger radii support more resonant wavelengths, they are also more susceptible to relative standard deviation. Similar to the absolute standard deviation, the process variation effect on the non-resonant wavelength regions remains relatively small.

Since the expected transmission efficiency at the through port shown in Figures 4.1 (b) – 4.5

(b) is complementary to the efficiency at the drop port of the same MRR under the same standard deviation, the troughs in the expected transmission efficiency spectra at the through port correspond to the peaks in the spectra at the drop port, and vice versa. If the influence of a different standard deviation on the peaks and troughs of the drop port inherently implies the corresponding influence on the troughs and peaks of the through port.

After presenting the distribution of the expected transmission efficiency and analyzing it, the optimization potential can be explained with the following example. Using the resonant wavelengths of 1504 nm, 1513.3 nm, and 1522.8 nm from the 10 μm MRR as benchmarks, Figure 4.1 shows that these three wavelengths correspond to the non-resonant wavelengths of the 27 μm MRR. This means that when the 10 μm MRR serves as the drop MRR and the 27 μm MRR serves as the through MRR in the transmission path of a signal, all three wavelengths are suitable choices. Since 1522.8 nm is closer to the resonance wavelength of the 27 μm MRR than the other two wavelengths and as the resonance peak broadens with increasing standard deviation, its expected transmission efficiency change at the drop port of 27 μm MRR is greater than the other two wavelengths. Therefore, 1522.8 nm is not an ideal choice for the signal when 10 μm MRR is the drop MRR, and 27 μm is the through MRR in this signal transmission path under process variation.

In summary, this chapter lays the groundwork for optimizing signal transmission efficiency, emphasizing the importance of determining the appropriate MRR radius and signal wavelength to counteract process variation in the network.

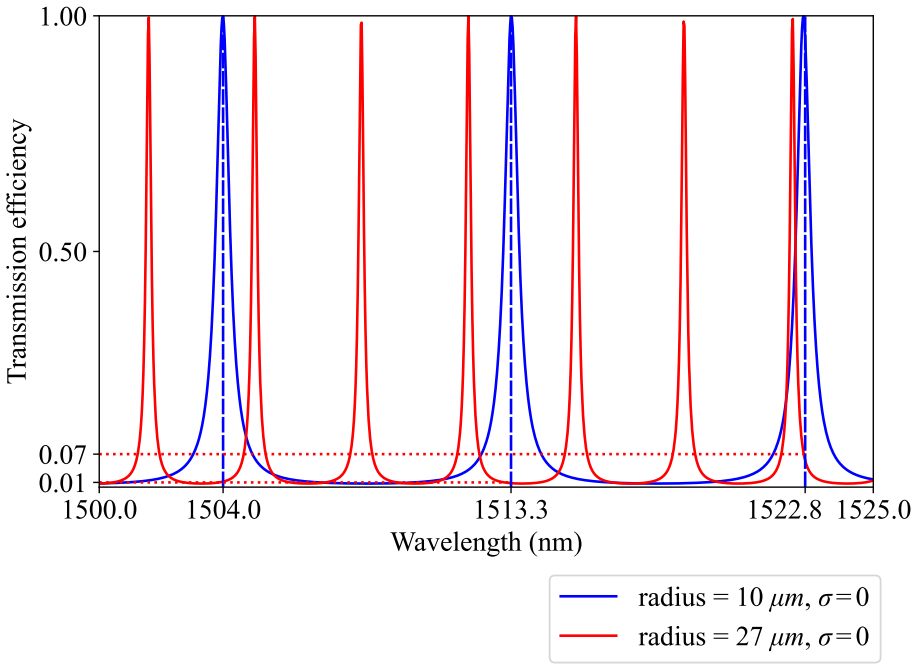

(a)

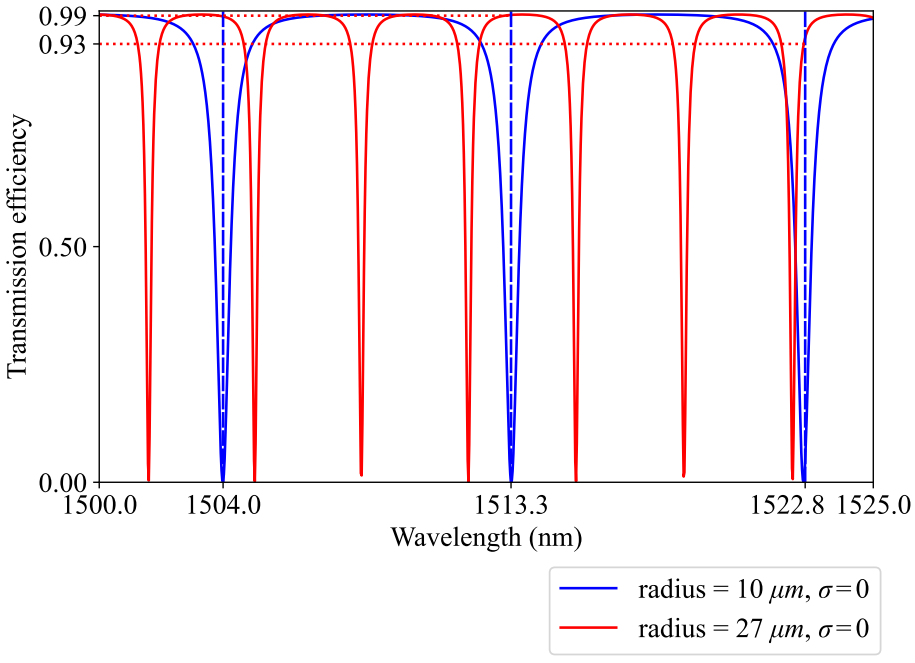

(b)

Figure 4.1.: (a) Transmission spectra at drop ports of MRRs without process variation. (b) Transmission spectra at through ports of MRRs without process variation.

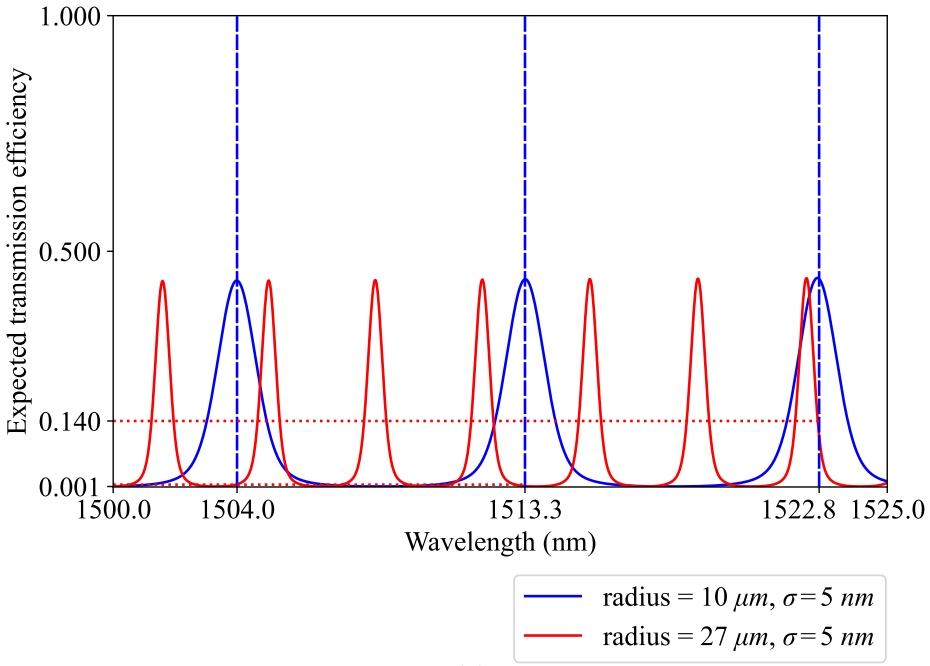

(a)

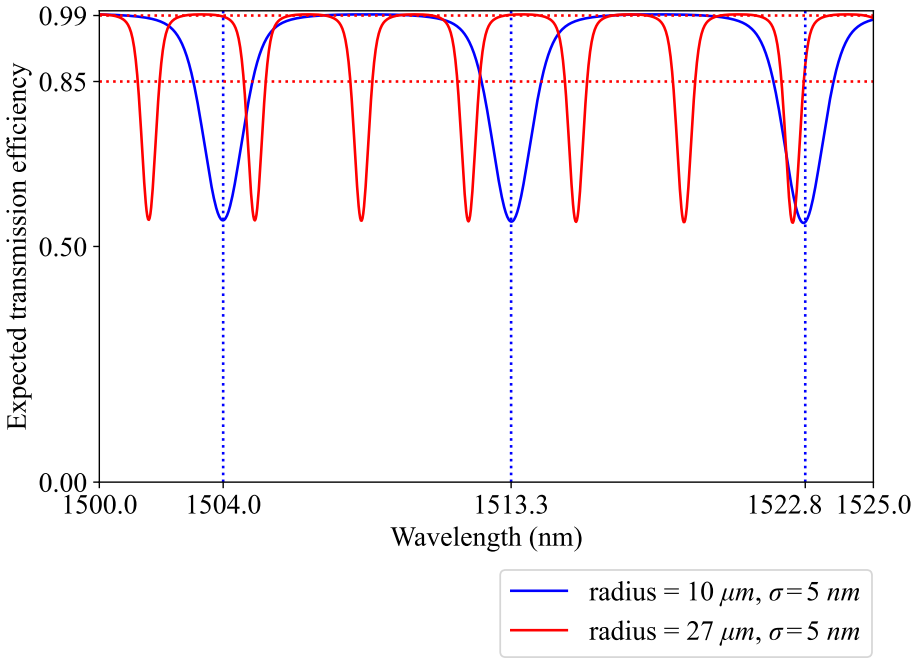

(b)

Figure 4.2.: (a) Expected transmission spectra at drop ports of MRRs with radii of 10 μm and 27 μm, each with a variation of 5 nm. (b) Expected transmission spectra at through ports of MRRs with radii of 10 μm and 27 μm, each with a variation of 5 nm.

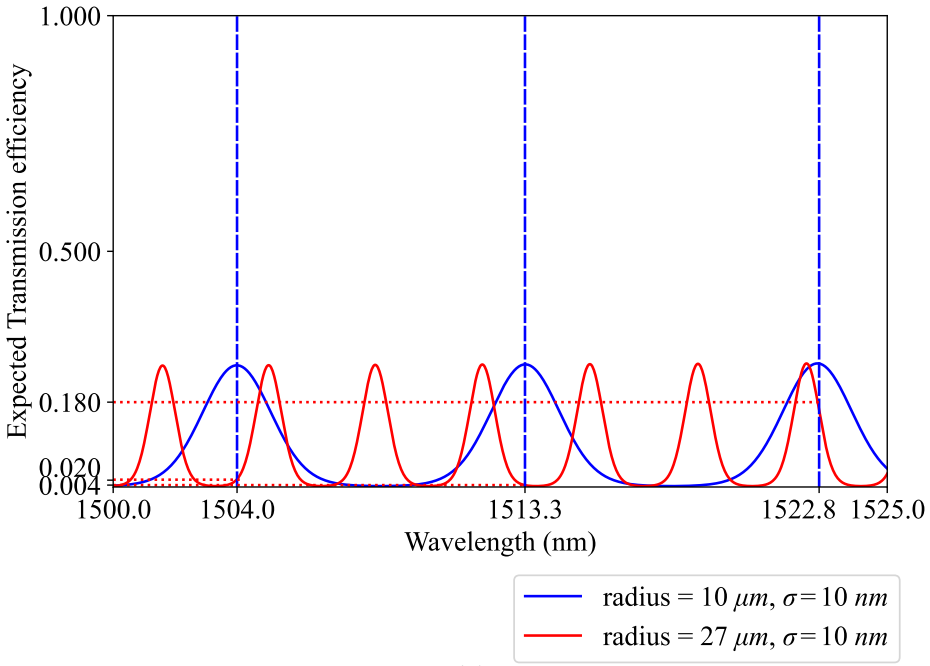

(a)

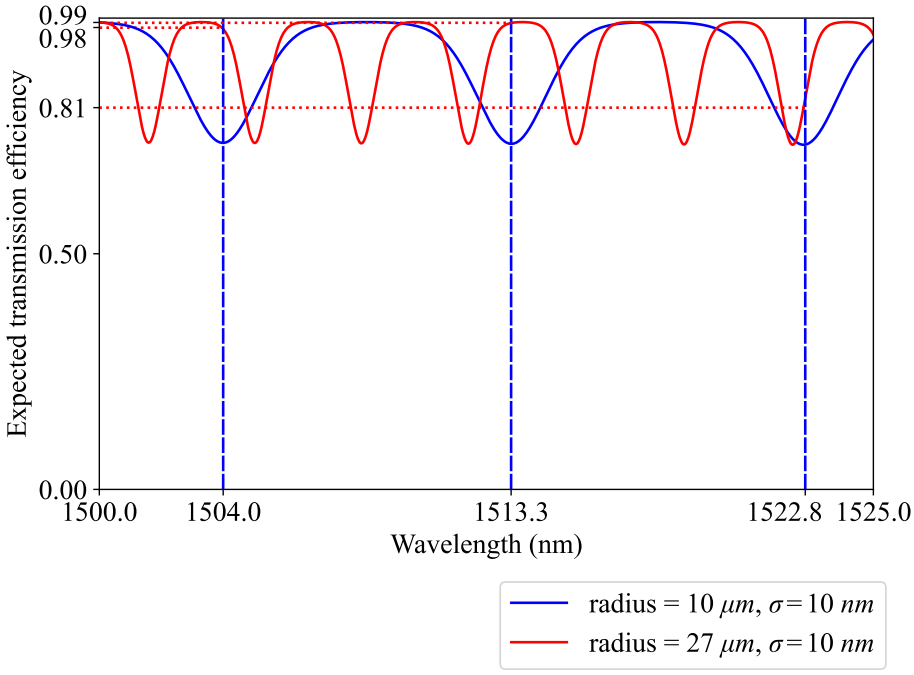

(b)

Figure 4.3.: (a) Expected transmission spectra at drop ports of MRRs with radii of 10 μm and 27 μm, each with a variation of 10 nm. (b) Expected transmission spectra at through ports of MRRs with radii of 10 μm and 27 μm, each with a variation of 10 nm.

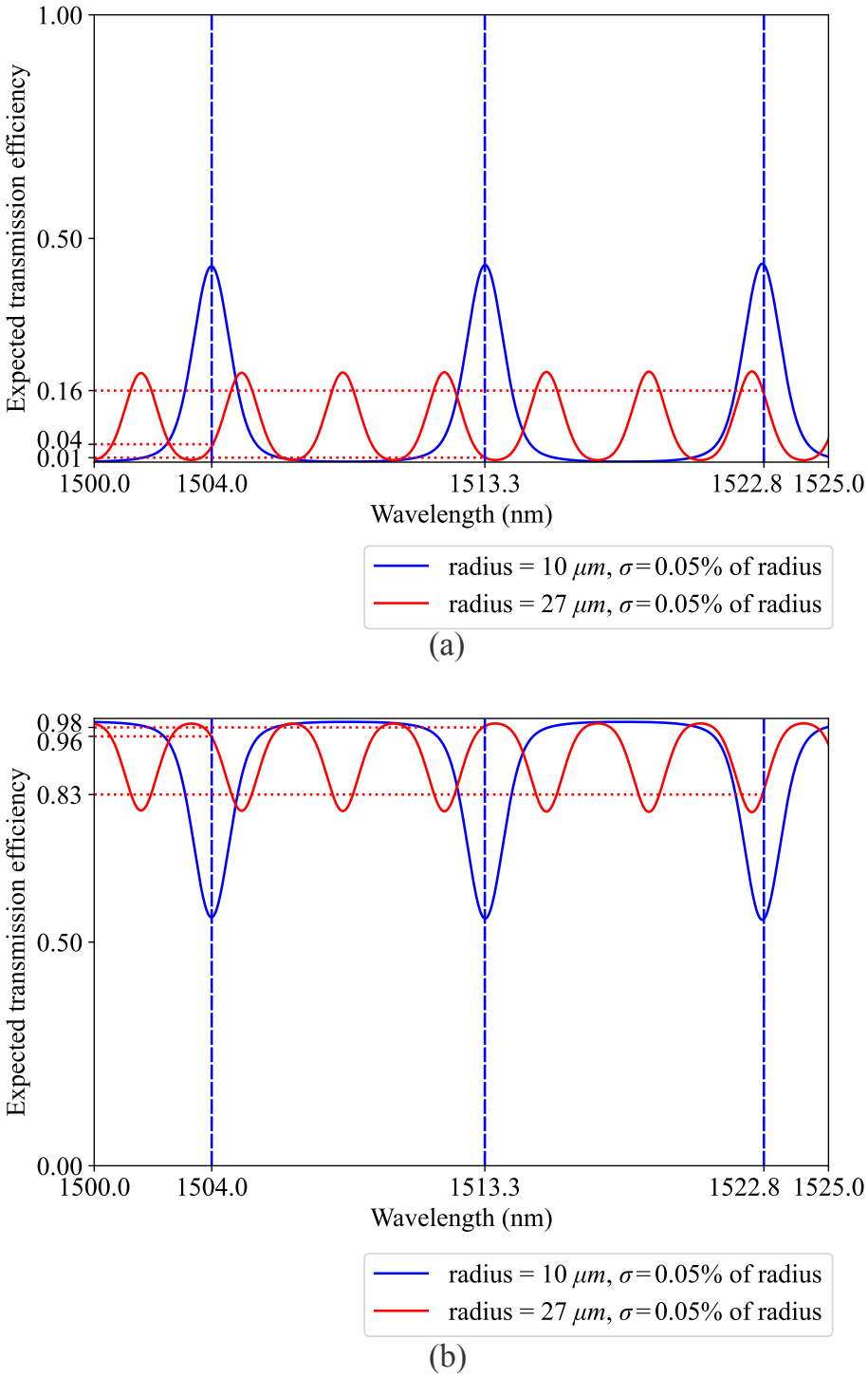

Figure 4.4.: (a) Expected transmission spectra at drop ports of MRRs with radii of 10 μm and 27 μm, each with a variation of 0.05% of their respective radius. (b) Expected transmission spectra at through ports of MRRs with radii of 10 μm and 27 μm, each with a variation of 0.05% of their respective radius.

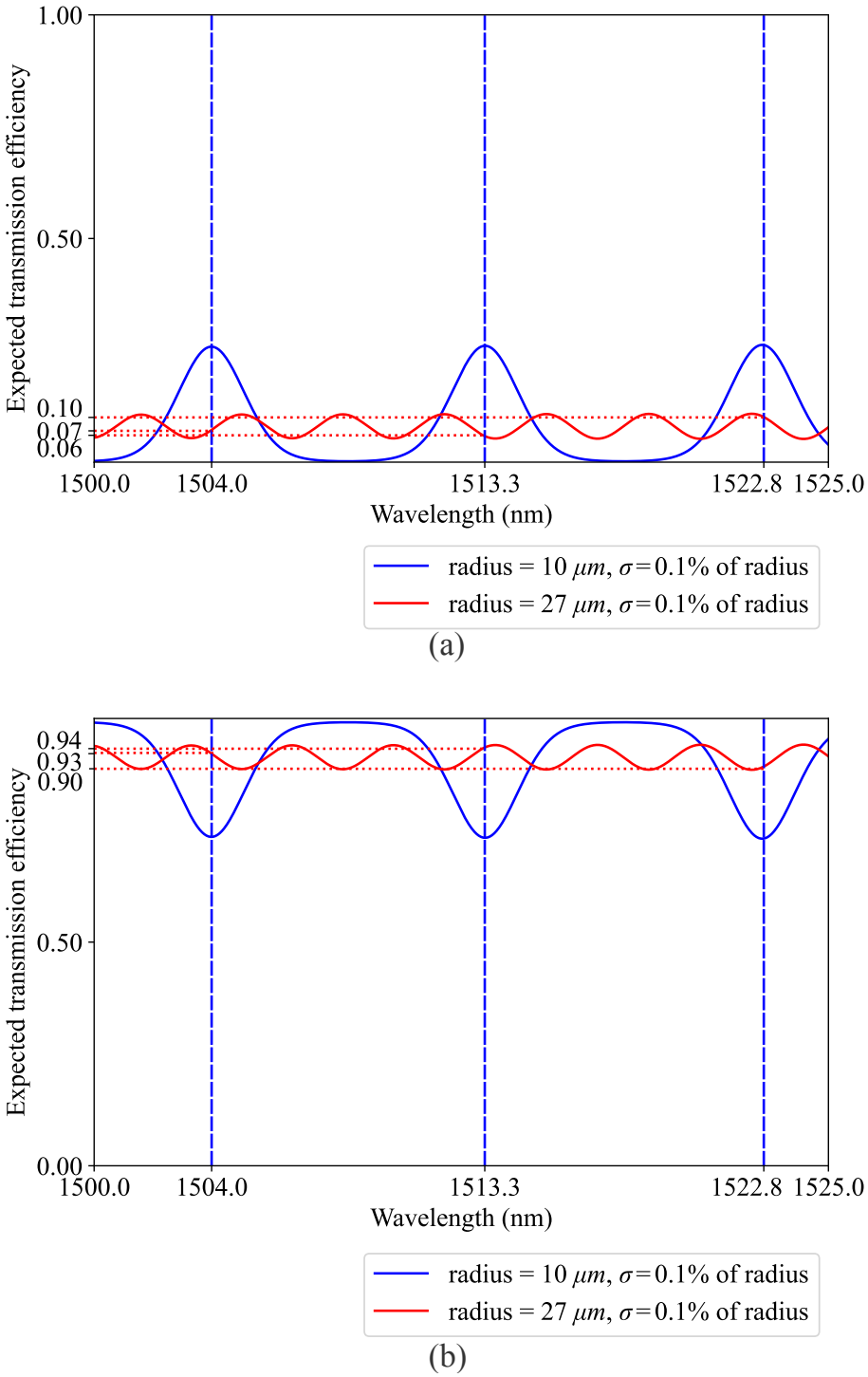

Figure 4.5.: (a) Expected transmission spectra at drop ports of MRRs with radii of 10 μm and 27 μm, each with a variation of 0.1% of their respective radius. (b) Expected transmission spectra at through ports of MRRs with radii of 10 μm and 27 μm, each with a variation of 0.1% of their respective radius.

5. Optimization Methods

This chapter discusses how to solve the optimization problem proposed in Chapter 3. First, I construct the integer linear programming (ILP) model for finding the global optimum. However, as the scale of the model increases, it becomes increasingly challenging within an acceptable runtime to solve the ILP model. Therefore, I develop a simulated annealing method specifically tailored for WRONoC. The experimental results show that this method can provide high-quality, optimized solutions within a practical problem-solving runtime.

5.1. Integer Linear Programming Model

In this section, I first review the definition and complexity of integer linear programming to provide the basic understanding necessary for the subsequent discussions. I then proceed to model the optimization problem using the principles of WRONoC and integer linear programming.

5.1.1. Theory and Complexity

Unless specifically stated otherwise, the concepts, definitions, and theorems discussed in this subsection are primarily a review of the content presented in (Korte & Vygen 2012).

Definition 5.1. Given a matrix $A \in \mathbb{Z}^{m \times n}$, vectors $\mathbf{b} \in \mathbb{Z}^m$, $\mathbf{c} \in \mathbb{Z}^n$, and a vector $\mathbf{x} \in \mathbb{Z}^n$, the integer linear programming (ILP) is an optimization problem defined as:

$$\begin{aligned} \text{maximize} \quad & \mathbf{c}^T \mathbf{x} \\ \text{subject to} \quad & A\mathbf{x} \leq \mathbf{b} \\ & \mathbf{x} \in \mathbb{Z}^n \end{aligned}$$

The task of ILP is to identify a **feasible solution**, represented by a vector $\mathbf{x} \in \mathbb{Z}^n$, that satisfies the constraint $A\mathbf{x} \leq \mathbf{b}$. Additionally, the solution should maximize the objective function $\mathbf{c}^T\mathbf{x}$. If a feasible solution achieves the maximum possible value of the objective function, it is referred to as an **optimal solution**.

The problem is said to be **infeasible** if the set of all $\mathbf{x} \in \mathbb{Z}^n$ satisfying $A\mathbf{x} \leq \mathbf{b}$ is empty, i.e., $\{x \in \mathbb{Z}^n : A\mathbf{x} \leq \mathbf{b}\} = \emptyset$.

The problem is said to be **unbounded** if for every $\mathbf{x} \in \mathbb{Z}^n$ satisfying $A\mathbf{x} \leq \mathbf{b}$, the objective function value $\mathbf{c}^T\mathbf{x}$ can become arbitrarily large, i.e., $\sup\{\mathbf{c}^T\mathbf{x} \mid \mathbf{x} \in \mathbb{Z}^n, A\mathbf{x} \leq \mathbf{b}\} = \infty$.

Definition 5.2. A decision problem is defined by a pair $\mathcal{P} = (X, Y)$, where X is the instance space that can be processed in polynomial time, and $Y \subseteq X$. The elements of Y are referred to as yes-instances, and the elements of $X \setminus Y$ are referred to as no-instances.

Definition 5.3. The set of decision problems that can be solved in polynomial time is denoted by P.

Definition 5.4. A decision problem $\mathcal{P} = (X, Y)$ belongs to NP (nondeterministic polynomial time) if there exists a polynomial p and another decision problem $\mathcal{P}' = (X', Y') \in P$, where $X' = \{x\#c : x \in X, c \in \{0,1\}^{\lfloor p(\text{size}(x))\rfloor}\}$. This implies that $Y = \{y \in X : \exists c \in \{0,1\}^{\lfloor p(\text{size}(y))\rfloor}$ with $y\#c \in Y'\}$. In this context, $x\#c$ is the concatenation of the string x, the symbol "#", and the string c. A string c that satisfies $y\#c \in Y'$ is designated as a certificate for y, since it verifies that y belongs to Y. An algorithm that solves $\mathcal{P}'$ is called a certificate-checking algorithm.

Proposition 5.5. *$P \subseteq NP$.*

Definition 5.6. Given two decision problems $\mathcal{P}_1 = (X_1, Y_1)$ and $\mathcal{P}_2 = (X_2, Y_2)$, $\mathcal{P}_1$ is said to polynomially transform to $\mathcal{P}_2$ if there exists a function $f : X_1 \to X_2$, which is computable in polynomial time, such that $f(x_1) \in Y_2$ for all $x_1 \in Y_1$, and $f(x_1) \in X_2 \setminus Y_2$ for all $x_1 \in X_1 \setminus Y_1$.

Definition 5.7. A decision problem $\mathcal{P} \in NP$ is referred to as NP-complete if every other decision problem in NP can be polynomially transformed to $\mathcal{P}$.

Definition 5.8. A decision problem is referred to as NP-hard if every problem in NP can be polynomially reduced to $\mathcal{P}$, meaning there exists a polynomial-time oracle algorithm for the problem in NP using $\mathcal{P}$.

Definition 5.9. Let X be a finite set of boolean variables. A **truth assignment** for X is a function $T : X \to \{\text{true, false}\}$. The **SAT problem** is defined for a given boolean formula. It aims to determine whether there exists a truth assignment for the variables of the boolean formula such that the entire formula evaluates to true.

Theorem 5.10 (Cook-Levin Theorem)**.** *SAT problem is NP-complete.*

The complexity of integer linear programming is given as follows:

Theorem 5.11. *Integer linear programming is NP-hard.*

Proof. An integer solution to an ILP can be used as a certificate, and it can be verified that this solution satisfies all the linear inequalities that constitute the ILP in polynomial time. Thus, the integer linear programming problem is in NP.

To show that ILP is NP-hard, a reduction of the well-known NP-complete problem SAT is performed. From Definition 5.9 and Theorem 5.10, it is known that an SAT instance is defined by a set of boolean variables and clauses and is NP-complete. An equivalent ILP instance can be constructed with the same number of variables. Each integer variable b_i is subjected to the constraint:

$$0 \leq b_i \leq 1. \tag{5.1}$$

For each clause in the SAT instance, an associated constraint is created in the ILP instance. For example, for the clause $x_1 \vee \neg x_2 \vee x_3$ in the SAT instance, the corresponding constraint in the ILP instance is

$$b_1 + (1 - b_2) + b_3 \geq 1. \tag{5.2}$$

This transformation can be done in polynomial time. Furthermore, it is straightforward to confirm that a satisfying assignment for the given SAT instance implies an integer solution for

the corresponding ILP instance and vice versa. For instance, it can be set $b_1 = 1$ or $b_2 = 0$, or $b_3 = 1$, which means $x_1 =$ true or $x_2 =$ false, or $x_3 =$ true in the truth assignment for SAT instance. Hence, the integer linear programming problem is NP-hard. □

5.1.2. Variable Setting

Having established the definitions and complexity, the ILP model is now developed to address the optimization problem proposed in Section 3.4. The input and design options for this model are adopted from Chapter 3 and Chapter 4.

I introduce a binary variable $b_{r_x,\lambda_l}^{(m_i,s_j),mrr_h}$ to represent whether wavelength λ_l is selected for signal (m_i, s_j) and mrr_h has a radius r_x, which can be interpreted as:

$$b_{r_x,\lambda_l}^{(m_i,s_j),mrr_h} = \begin{cases} 1, & \text{if wavelength } \lambda_l \text{ is selected for signal } (m_i, s_j) \text{ and } mrr_h \text{ has radius } r_x, \\ 0, & \text{otherwise.} \end{cases} \tag{5.3}$$

This representation can demonstrate the selection of radius and wavelength under the optimization objective. If the binary variable takes the value 1, it indicates that signal (m_i, s_j) is transmitted on wavelength λ_l, and the MRR with index h has a radius of r_x. Conversely, if the value of this variable is 0, it means that no wavelength λ_l has been selected for the signal (m_i, s_j) or no radius r_x has been selected for the MRR with index h.

5.1.3. Radii and Wavelength Assignment

To ensure that exactly one wavelength is selected for each signal and exactly one radius is assigned to each MRR in the given topology, this constraint can be expressed as follows:

$$\forall (m_i, s_j) \in \mathcal{SP},\ \forall mrr_h \in \mathcal{MRR}:$$

$$\sum_{r_x \in \mathcal{R}} \sum_{\lambda_l \in \Lambda} b_{r_x,\lambda_l}^{(m_i,s_j),mrr_h} = 1. \tag{5.4}$$

For example, if $b_{r_a,\lambda_b}^{(m_i,s_j),mrr_h}$ is set to 1, this constraint ensures that

$$\forall r_x \in \mathcal{R} \setminus \{r_a\},\ \forall \lambda_l \in \Lambda \setminus \{\lambda_b\} :\ b_{r_x,\lambda_l}^{(m_i,s_j),mrr_h} = 0.$$

This implies that this signal (m_i, s_j) is assigned only one wavelength λ_b and that mrr_h has only one radius r_a.

5.1.4. Consistent Wavelength Selection

To ensure a consistent signal wavelength transmitted in a path, I designate the first MRR in $\mathcal{MRR}_{(m_i,s_j)}$, denoted as $mrr_0^{(m_i,s_j)}$, as the benchmark. All other MRRs in the same transmission path of signal (m_i, s_j) must cooperate in selecting and switching the same wavelength as $mrr_0^{(m_i,s_j)}$. This constraint is modeled as follows:

$$\forall (m_i, s_j) \in \mathcal{SP},\ \forall mrr_h \in \mathcal{MRR}_{(m_i,s_j)} \setminus \{mrr_0^{(m_i,s_j)}\},\ \forall \lambda_l \in \Lambda :$$

$$\sum_{r_x \in \mathcal{R}} b_{r_x,\lambda_l}^{(m_i,s_j),mrr_0^{(m_i,s_j)}} - \sum_{r_y \in \mathcal{R}} b_{r_y,\lambda_l}^{(m_i,s_j),mrr_h} = 0. \tag{5.5}$$

The summation terms, $\sum_{r_x \in \mathcal{R}} b_{r_x,\lambda_l}^{(m_i,s_j),mrr_0^{(m_i,s_j)}}$ and $\sum_{r_y \in \mathcal{R}} b_{r_y,\lambda_l}^{(m_i,s_j),mrr_h}$, consider the entire range of radius options for the $mrr_0^{(m_i,s_j)}$ and mrr_h. By ensuring that $mrr_0^{(m_i,s_j)}$ and mrr_h have actually chosen radii for themselves, it becomes possible to assess whether the signal (m_i, s_j) has chosen the wavelength λ_l. If the signal (m_i, s_j) selects the wavelength λ_l, then

$$\sum_{r_x \in \mathcal{R}} b_{r_x,\lambda_l}^{(m_i,s_j),mrr_0^{(m_i,s_j)}} = \sum_{r_y \in \mathcal{R}} b_{r_y,\lambda_l}^{(m_i,s_j),mrr_h} = 1.$$

Combining the Equation (5.4) yields

$$\forall \lambda_p \in \Lambda \setminus \{\lambda_l\} : \sum_{r_x \in \mathcal{R}} b_{r_x,\lambda_p}^{(m_i,s_j),mrr_0^{(m_i,s_j)}} = \sum_{r_y \in \mathcal{R}} b_{r_y,\lambda_p}^{(m_i,s_j),mrr_h} = 0,$$

which means that no wavelength other than λ_l will be selected for signal (m_i, s_j). This ensures that the wavelength transmitted along the path of signal (m_i, s_j) remains consistent.

5.1.5. Consistent Radius Selection

An MRR can appear in multiple signal transmission paths, but its radius must remain consistent. I denote the set of signals whose transmission paths contain mrr_h as $\mathcal{SP}_{mrr_h}$ and the first element in this set as $sp_0^{mrr_h}$. The $sp_0^{mrr_h}$ is used as the benchmark. The radius of mrr_h in other transmission paths of signals within $\mathcal{SP}_{mrr_h}$ must be the same as the radius of mrr_h in $sp_0^{mrr_h}$. The constraint can be modeled as follows:

$$\forall mrr_h \in \mathcal{MRR},\ \forall (m_i, s_j) \in \mathcal{SP}_{mrr_h} \setminus \{sp_0^{mrr_h}\},\ \forall r_x \in \mathcal{R}\ :$$

$$\sum_{\lambda_l \in \Lambda} b_{r_x,\lambda_l}^{sp_0^{mrr_h},mrr_h} - \sum_{\lambda_p \in \Lambda} b_{r_x,\lambda_p}^{(m_i,s_j),mrr_h} = 0. \tag{5.6}$$

The summation terms, $\sum_{\lambda_l \in \Lambda} b_{r,\lambda_l}^{(m_i,s_j),mrr_h}$ and $\sum_{\lambda_p \in \Lambda} b_{r_x,\lambda_p}^{sp_0^{mrr_h},mrr_h}$, consider the entire range of wavelength options for the signal (m_i, s_j) and $sp_0^{mrr_h}$. By ensuring that the signal (m_i, s_j) and $sp_0^{mrr_h}$ have actually chosen wavelengths for themselves, it becomes possible to assess whether the mrr_h has chosen the radius r_x. If the mrr_h selects the radius r_x, then

$$\sum_{\lambda_l \in \Lambda} b_{r_x,\lambda_l}^{(m_i,s_j),mrr_h} = \sum_{\lambda_p \in \Lambda} b_{r_x,\lambda_p}^{sp_0^{mrr_h},mrr_h} = 1.$$

Combining the Equation (5.4) yields

$$\forall r_y \in \mathcal{R} \setminus \{r_x\} : \sum_{\lambda_l \in \Lambda} b_{r_y,\lambda_l}^{(m_i,s_j),mrr_h} = \sum_{\lambda_p \in \Lambda} b_{r_y,\lambda_p}^{sp_0^{mrr_h},mrr_h} = 0,$$

which means that mrr_h will not have a radius other than r_x. This ensures that the radius of each MRR remains the same in this topology.

5.1.6. Expected Value Maximization

The expected transmission efficiency in dB at the drop port of each $mrr_h \in \mathcal{MRR}$ can be denoted as $\mathbb{E}[H_{\text{drop}}^{(m_i,s_j),mrr_h}]_{\text{dB}}$ and modeled from the selected radius and wavelength using the following constraint:

$$\mathbb{E}[H_{\text{drop}}^{(m_i,s_j),mrr_h}]_{\text{dB}} = \sum_{r_x \in \mathcal{R}} \sum_{\lambda_l \in \Lambda} \left(b_{r_x,\lambda_l}^{(m_i,s_j),mrr_h} \times \mathbb{E}[H_{\text{drop}}(R_x, \lambda_l)]_{\text{dB}} \right). \tag{5.7}$$

Similarly, the expected transmission efficiency of signal (m_i, s_j) at the through port of $mrr_h \in \mathcal{MRR}$ can be denoted as $\mathbb{E}[H_{\text{through}}^{(m_i,s_j),mrr_h}]_{\text{dB}}$ and expressed with the following constraint:

$$\mathbb{E}[H_{\text{through}}^{(m_i,s_j),mrr_h}]_{\text{dB}} = \sum_{r_x \in \mathcal{R}} \sum_{\lambda_l \in \Lambda} \left(b_{r_x,\lambda_l}^{(m_i,s_j),mrr_h} \times \mathbb{E}[H_{\text{through}}(R_x, \lambda_l)]_{\text{dB}} \right), \tag{5.8}$$

where $R_x \sim N(r_x, \sigma^2)$. Since the constraint in Equation (5.4) ensures that only one radius and wavelength combination is selected, this summation will have only one non-zero term and practically takes the expected transmission efficiency corresponding to the selected radius and wavelength for the given MRR at the drop and through port.

Using Theorem 3.8, the expected transmission efficiency in dB of signal (m_i, s_j) can be denoted as $\mathbb{E}[H_{(m_i,s_j)}]_{\text{dB}}$ and is constrained by the following:

$$\begin{aligned} \mathbb{E}[H_{(m_i,s_j)}]_{\text{dB}} = & \sum_{mrr_h \in \mathcal{MRR}_{(m_i,s_j)}^{\text{drop}}} \mathbb{E}[H_{\text{drop}}^{(m_i,s_j),mrr_h}]_{\text{dB}} \\ & + \sum_{mrr_f \in \mathcal{MRR}_{(m_i,s_j)}^{\text{through}}} \mathbb{E}[H_{\text{through}}^{(m_i,s_j),mrr_h}]_{\text{dB}} \\ & + c_{(m_i,s_j)} \cdot (1 - cl)_{\text{dB}}, \end{aligned} \tag{5.9}$$

where $c_{(m_i,s_j)}$ represents the number of waveguide crossing and cl is the crossing coefficient.

Based on the above constraints, the worst-case expected transmission efficiency in dB of all signals, denoted as $\mathbb{E}[H_{\text{worst}}]_{\text{dB}}$, is modeled with the following constraint:

$$\forall (m_i, s_j) \in \mathcal{SP} : \ \mathbb{E}[H_{\text{worst}}]_{\text{dB}} \leq \mathbb{E}[H_{(m_i,s_j)}]_{\text{dB}} \tag{5.10}$$

This constraint ensures that for each signal (m_i, s_j) in the set of all possible signals $\mathcal{SP}$, the worst-case expected transmission efficiency, $\mathbb{E}[H_{\text{worst}}]_{\text{dB}}$, must be less than or equal to the expected transmission efficiency of each signal in the topology.

Thus, the optimization model can be formulated as follows:

$$\begin{aligned} &\text{Maximize:} \quad \mathbb{E}[H_{\text{worst}}]_{\text{dB}}, \\ &\text{Subject to:} \quad (5.3) - (5.10). \end{aligned}$$

5.2. Simulated Annealing

Since the integer linear programming problem is proved to be an NP-hard problem, finding the exact solution in finite time becomes extremely difficult as the problem size increases. On the contrary, metaheuristic algorithms have been widely used for their ability to quickly give high-quality, feasible solutions. In the context of global optimization, relying only on local optimization does not guarantee that a globally optimal solution will be found. Simulated annealing, a type of metaheuristic algorithm, addresses this issue. It's a random optimization method that not only accepts solutions with better objective function values but also incorporates a probabilistic mechanism to accept solutions with worse objective function values. In the course of this process, the probability of accepting worse solutions is gradually decreased to zero. This allows the search process to escape local minima and fully explore the global solution space. As stated in (Dekkers & Aarts 1991), this algorithm converges asymptotically to the global optimum.

The implementation of the algorithm requires the following parameters:

T_{init}: The initial temperature.

T_{current}: The current temperature in the annealing schedule.

T_{stop}: The stopping temperature.

α : The cooling rate.

P_{accept}: The acceptance probability.

N_{iter}: The total number of iterations performed by the algorithm. Each iteration represents a complete cycle of the optimization process.

$\mathcal{V}_{\text{neigh}}$: The set of neighboring solutions.

N_{init}: The number of initial solutions.

$\mathcal{V}_{\text{init}}$: The set of Initial solutions.

$N_{\text{no\_improve}}$: The monitor for stagnation in the optimization process.

In (Dekkers & Aarts 1991), the classic implementation of the simulated annealing algorithm is laid out as follows:

Step 1: The initial solution, $\mathcal{V}_{\text{init}}$, is set together with the initial temperature, T_{init}. The current temperature is then assigned as $T_{\text{current}} = T_{\text{init}}$.

Step 2: For each initial solution, the following steps are repeated until the stopping condition is met:

- A neighboring solution is generated from the set $\mathcal{V}_{\text{neigh}}$ of the current solution.
- The objective function for this neighboring solution is evaluated.
- If the neighboring solution is better than the current solution, it will be accepted as the new current solution. However, if the neighbor solution is inferior to the current solution, it can still be accepted as the new current solution with probability $P_{\text{accept}} = \exp(-\Delta f / T_{\text{current}})$, where Δf is the difference between the objective function values of the neighbor solution and the current solution.

Step 3: The temperature T_{current} is decreased according to the cooling rate, α.

Step 4: The best solution found is returned once the stopping condition is met.

In this classic simulated annealing process, the algorithm uses a temperature-dependent iterative process that simulates the cooling process in metallurgical annealing. This includes a defined acceptance mechanism that probabilistically accepts sub-optimal solutions with an acceptance probability of $P_{\text{accept}} = \exp(-\Delta f / T_{\text{current}})$. This probability decreases as the difference increases and also as the current temperature decreases. In contrast to the setting of the acceptance probability in the classical algorithm, in this work, the setting of the acceptance probability is related to the current expected transmission efficiency value as well as the current temperature, based on the property that the transmission efficiency takes values between [0,1]. Next, I will explain how this algorithm can be specifically applied to the optimization problem in this work.

5.2.1. Preparation of Initial Solutions

Initial solution generation is the starting point of the algorithm. This process consists of assigning a random radius to each MRR and a wavelength to each signal, then generating the initial solution set based on the number of initial solutions. It begins by introducing the parameters required for the optimization process:

$v \in \mathcal{V}_{\text{init}}$: A single initial solution, represented as a vector, where each element specifies the radius for each MRR and the wavelength used for data transmission in each signal path.

From the available wavelength options, I filter the wavelengths that can be transmitted with high efficiency to reach the "drop" and "through" ports of an MRR with a given radius without process variation, and categorize these wavelengths into two sets:

$\Lambda_{\text{drop},r_x}$: The set of wavelengths selected from the available wavelength options that satisfy the condition $H_{\text{drop}}(r_x, \lambda_l) \geq p$ for a given MRR with radius r_x, where $p \in [0, 1]$ represents the criteria for filtering high efficiency.

$\Lambda_{\text{through},r_y}$: The set of wavelengths from the available wavelength options that satisfy the condition $H_{\text{through}}(r_y, \lambda_l) \geq q$ for a given MRR with radius r_y, where $q \in [0, 1]$ represents the criteria for filtering high efficiency.

The following are the steps involved in the preparation of the initial solutions for the simulated annealing algorithm tailored to the optimization problem in this work:

Step 1: Depending on the number of initial solutions N_{init} specified in the input, a random radius is assigned to each MRR in each initial solution.

Step 2: To speed up the optimization, the signal wavelengths can be selected based on given MRR radii. The purpose of the selection is to allow the signal to be efficiently transmitted to the drop port of the drop MRR and the through port of the through MRR. Therefore, it is possible to create a set of wavelengths $\Lambda_{(m_i,s_j)}$ as candidate wavelengths for each signal. The selection process can be decomposed into three cases:

- The transmission path of signal (m_i, s_j) contains only drop MRRs: The wavelength

set is defined as $\Lambda_{(m_i,s_j)} = \bigcap_{mrr_h \in \mathcal{MRR}^{\text{drop}}_{(m_i,s_j)}} \Lambda_{\text{drop},r_x}$, where r_x is the radius of mrr_h.

- The transmission path of signal (m_i, s_j) contains only through MRRs: The wavelength set is defined as $\Lambda_{(m_i,s_j)} = \bigcap_{mrr_f \in \mathcal{MRR}^{\text{through}}_{(m_i,s_j)}} \Lambda_{\text{through},r_y}$, where r_y is the radius of mrr_f.

- The transmission path of signal (m_i, s_j) contains drop and through MRRs: The set is defined as $\Lambda_{(m_i,s_j)} = \left(\bigcap_{mrr_h \in \mathcal{MRR}^{\text{drop}}_{(m_i,s_j)}} \Lambda_{\text{drop},r_x}\right) \cap \left(\bigcap_{mrr_f \in \mathcal{MRR}^{\text{through}}_{(m_i,s_j)}} \Lambda_{\text{through},r_y}\right)$. If $\Lambda_{(m_i,s_j)} = \emptyset$, then $\Lambda_{(m_i,s_j)} = \bigcap_{mrr_h \in \mathcal{MRR}^{\text{drop}}_{(m_i,s_j)}} \Lambda_{\text{drop},r_x}$, where r_x is the radius of mrr_h and r_y is the radius of mrr_f.

Step 3: For each signal (m_i, s_j), the wavelengths in $\Lambda_{(m_i,s_j)}$ are iterated. Based on the current configuration of each MRR and the given standard deviation, the expected transmission efficiency of signal (m_i, s_j) on each wavelength is calculated using Definition 3.6, then the wavelength that maximizes the expected transmission efficiency is selected as the initial wavelength for signal (m_i, s_j).

These steps complete the configuration of the initial solutions. Each initial solution now has a radius assigned to each MRR and a wavelength selected for each signal.

5.2.2. Optimization Process

Following the preparation of the initial solution, the optimization process begins. During each iteration of the optimization process, a solution is generated based on the outcome of the previous iteration. Solutions from previous iterations are labeled as **old**, while those generated in the current iteration are labeled as **new**. The following steps explain the process in detail:

Step 1: Based on the current solutions, the radius of each MRR is denoted by $r_{mrr_h,\text{old},k}$ and the wavelength for signal (m_i, s_j) is represented by $\lambda_{(m_i,s_j),\text{old},k}$, where k represents the k-th solution. The expected transmission efficiency of each signal for each solution is evaluated using Definition 3.6. Thus, the signal with the lowest expected transmission efficiency can be determined. This signal is denoted as $sp_{\text{worst,old},k}$ and its expected transmission

efficiency is denoted as $\mathbb{E}[H_{\text{worst,old},k}]$.

Step 2: The MRR with the lowest expected transmission efficiency in the transmission path of $sp_{\text{worst,old},k}$ is found and denoted as $mrr_{\text{worst},k}$. A new radius for $mrr_{\text{worst},k}$ is chosen randomly from the radii options.

Step 3: All signals whose transmission paths contain $mrr_{\text{worst},k}$ are identified and denoted as a set $\mathcal{SP}_{mrr_{\text{worst},k}}$. Based on the new radius of $mrr_{\text{worst},k}$, following the same methodology as **Step 2** and **Step 3** in the Section 5.2.1, new wavelengths are assigned to these signals in $\mathcal{SP}_{mrr_{\text{worst},k}}$. The radius of $mrr_{\text{worst},k}$ is denoted by $r_{mrr_{\text{worst},k},\text{new}}$ and the new wavelength for signals of $\mathcal{SP}_{mrr_{\text{worst},k}}$ is represented by $\lambda_{(m_x,s_y),\text{new},k}$, where $(m_x, s_y) \in \mathcal{SP}_{mrr_{\text{worst},k}}$.

Step 4: The expected transmission efficiency of each signal can be determined based on the new MRR radii and signal wavelengths. The signal with the new lowest expected transmission efficiency of k-th solution is expressed as $sp_{\text{worst,new},k}$. Its expected transmission efficiency is denoted by $\mathbb{E}[H_{\text{worst,new},k}]$.

Step 5: $\mathbb{E}[H_{\text{worst,new},k}]$ is compared with $\mathbb{E}[H_{\text{worst,old},k}]$, and the results are evaluated in two cases:

- If $\mathbb{E}[H_{\text{worst,new},k}] > \mathbb{E}[H_{\text{worst,old},k}]$, the radius solution $r_{mrr_{\text{worst},k},old}$ is set to the same as $r_{mrr_{\text{worst},k,\text{new}}}$, the wavelength solution $\lambda_{(m_x,s_y),\text{old},k}$ is set to the same as $\lambda_{(m_x,s_y),\text{new},k}$ and $\mathbb{E}[H_{\text{worst,old},k}]$ is set to the same as $\mathbb{E}[H_{\text{worst,new},k}]$.

- If $\mathbb{E}[H_{\text{worst, new},k}] \leq \mathbb{E}[H_{\text{worst, old},k}]$, the new solution is accepted with a probability given by:

$$P_{\text{accept},k} = \mathbb{E}[H_{\text{worst,new},k}] \times T_{\text{current}}. \tag{5.11}$$

  If accepted, the radius solution $r_{mrr_{\text{worst},k},old}$ is set to the same as $r_{mrr_{\text{worst},k},\text{new}}$, the wavelength solution $\lambda_{(m_x,s_y),\text{old},k}$ is set to the same as $\lambda_{(m_x,s_y),\text{new},k}$ and $\mathbb{E}[H_{\text{worst,old},k}]$ is set to the same as $\mathbb{E}[H_{\text{worst,new},k}]$. If not accepted, the radius solution $r_{mrr_{\text{worst},k},\text{old}}$, the wavelength solution $\lambda_{(m_x,s_y),\text{old},k}$, and the worst expected transmission efficiency $\mathbb{E}[H_{\text{worst,old},k}]$ do not change.

Step 6: After each iteration, the $\mathbb{E}[H_{\text{worst,old},k}]$ values of all solutions are compared. The highest

expected transmission efficiency of all solutions is denoted as $\mathbb{E}[H_{\text{worst}}]$. After a certain number of iterations, a part of the solutions with lower $\mathbb{E}[H_{\text{worst,old},k}]$ are discarded, while those with higher $\mathbb{E}[H_{\text{worst,old},k}]$ are further optimized. This enables that in the early stages of optimization, the algorithm performs a global search to explore a wide range of possible solutions. In the later stages, the algorithm performs a local search on solutions with better $\mathbb{E}[H_{\text{worst,old},k}]$, which improves computational efficiency.

Step 7: The number of iterations is increased by one. The current temperature T_{current} is lowered based on the cooling schedule α. As the temperature decreases, the probability of accepting a worse solution also decreases, so the algorithm tends to perform a local search to find the local optimum. If the stopping condition has not been reached, the algorithm returns to Step 1. If the stopping condition is achieved, the process is terminated.

Step 8: The $\mathbb{E}[H_{\text{worst}}]_{\text{dB}}$ is calculated based on the $\mathbb{E}[H_{\text{worst}}]$ using Definition 3.9.

In **Step 5** of the optimization process, the probability of accepting a worse solution is determined by the new worst expected transmission efficiency, which ranges from 0 to 1, and the current temperature. Both the initial temperature and the cooling rate are set to be less than 1, ensuring that the current temperature and the acceptance probability also range from 0 to 1. In the initial stages of optimization, with a high current temperature, there's a relatively high probability of accepting a new solution, even if its worst transmission efficiency value is lower. This avoids limiting the search to the vicinity of the old solution and allows a global search. In the later stages of optimization, when the new expected transmission efficiency is lower, and the temperature is decreased, the acceptance probability is also lower. Then, the algorithm avoids accepting the new, worse solution and focuses on local search with the neighborhood of the old solution. Since the solution in the later stages tends to be relatively better, they provide an efficient starting point for local search, thus avoiding redundant optimization efforts on a worse solution. In summary, this strategy ensures global exploration of the optimization space early in the process while increasing efficiency in the later stages.

In **Step 7**, two stopping conditions are set:

- The first condition is that when the maximum iteration count N_{iter} is reached.

- The second stopping condition is that if $\mathbb{E}[H_{\text{worst}}]$ of all solutions does not change after

several consecutive iterations.

5.2.3. Algorithm Summary

The optimization process improves the solution by adjusting the MRR radii and the signal wavelengths. This algorithm accepts worse solutions with a certain probability while incorporating stopping conditions and allows a wide range of solution space exploration to maximize the worst expected transmission efficiency over all signals on a global scale.

Finally, the optimization objective of this algorithm can be formulated as:

$$\text{Maximize:} \quad \mathbb{E}[H_{\text{worst}}]_{\text{dB}}.$$

6. Experimental Results

This chapter details the experimental setup and presents a comprehensive analysis of the results.

6.1. Inputs and Parameter Settings

This approach is implemented in C++ on a computer equipped with an Apple M1 Pro 10-core CPU and applied to two WRONoC topologies of different scales: Light (Zheng et al. 2021) and Snake (Ramini et al. 2013).

Assume that all MRRs in a given topology suffer from the same process variation. The absolute standard deviations are set to 1 nm, 2 nm, 5 nm, and 10 nm, while the relative standard deviations are set to 0.01%, 0.02%, 0.05%, and 0.1% of each radius option. When there is no process variation, the standard deviation is set to 0.

To compute the expected transmission efficiency for various radius-wavelength combinations under different standard deviations, I use the same setup as for the empirical analysis in Chapter 4. The cross-coupling coefficient k is set to 0.4. This value then determines the self-coupling coefficient t, which is calculated via the relation $t = \sqrt{1 - k^2} = \sqrt{0.84}$. I divide the domains of the expected value functions into 1000 equal intervals and use the Riemann sum method for approximation. The crossing loss coefficient is set to 0.009168 for the experiments of the integer linear programming model and the simulated annealing algorithm.

To solve the integer linear programming model, I use an optimization solver called Gurobi (Gurobi Optimization, LLC 2023). As described in (Li, Tseng, Tala & Schlichtmann 2020), I evaluate the transmission efficiency at the drop port for radius values from 5 μm to 30 μm in steps of 0.25 μm and for wavelengths from 1500 nm to 1600 nm in steps of 0.8 nm. Any radius-

wavelength combination yielding a transmission efficiency greater than 0.995 at the drop port is selected. As a result, I select 38 radii and 33 wavelengths as input options for the ILP model and test the model in the Light 4×3 and Snake 4×4 topologies. When the network topologies are extended to Light 8×7 and Snake 8×8, the solver cannot complete the solution within 10 hours using the current radius and wavelength options. Therefore, to solve the problem on a larger scale, I further expand the range of radii, wavelengths, and topology scales and conduct an experiment using the simulated annealing algorithm.

In the simulated annealing experiment, as described in (Li, Tseng, Tala & Schlichtmann 2020), I specify the radius range from 5 μm to 30 μm with a smaller increment of 0.025 μm for a total of 1001 different radius options. I define a band of available wavelengths between 1500 nm and 1600 nm with a smaller increment of 0.1 nm, providing 1001 different wavelength options. These settings allow the calculation of the expected values of the transmission efficiency at the drop port and through port for each of the 1002001 radius-wavelength combinations at each standard deviation setting. Storing the calculated expected value allows direct access to the expected values in the optimization process, eliminating the need for repetitive calculations.

The parameters of the simulated annealing algorithm and their corresponding values are shown in Table 6.1.

Table 6.1.: Simulated annealing parameters

Parameter	Description	Value
T_{init}	Initial temperature	1
N_{init}	Number of initial solutions	100
α	Cooling rate	0.99
p	Selection criteria for $\Lambda_{\text{drop},r_x}$	0.85
q	Selection criteria for $\Lambda_{\text{through},r_y}$	0.85
$N_{\text{no\_improve}}$	Consecutive number of no improvement	1000
N_{iter}	Maximum number of iterations	3000

Specifically, I define $N_{\text{no\_improve}}$ to be 1000. I start counting the consecutive iterations where no better solution is found from zero, so when the count reaches $N_{\text{no\_improve}}$, it actually means that consecutive 1001 iterations have been completed without any improvement, and the search will terminate early. Since this number coincides with the number of radius options, it can be assumed that the algorithm has probably found an optimal solution or is stuck in a local optimum. It is time-consuming and inefficient to continue randomly finding a new radius for

the MRR with the worst performance.

The number of initial solutions N_{init} is set to 100. The purpose of this is to provide more starting points for the search, expand the search space, and reduce the randomness of the final solution. Given that the initial solutions in the algorithm are generated randomly, to ensure the fairness of the experiment, I utilize the same set of 100 initial solutions for optimization under all standard deviations.

From the 50th to the 140th iteration in the simulated annealing algorithm, five poor-quality solutions are discarded every ten iterations. Thus, after the 140th iteration, only five high-quality solutions continue to be optimized until the algorithm reaches its stopping conditions. This strategy improves the overall efficiency of the optimization process because it globally explores solutions in the early stages of optimization and then focuses on high-quality solutions for local optimization in the later stages.

Two experimental designs are set up for comparative analysis. The first design is called the **nominal design**. It is optimized under condition where process variation is not considered (i.e., $\sigma = 0$). The goal of this design is to maximize the worst-case transmission efficiency of the signal, where the MRRs in the topology are not affected by process variation, and to optimize the selection of MRR radii and signal wavelengths. The second design is called the **variation-aware design**. It takes process variation (i.e., $\sigma \neq 0$) into account. The goal is to maximize the worst-case expected transmission efficiency of the signal, where the MRRs in the topology are affected by process variation, and to optimize the selection of MRR radii and signal wavelengths for a given standard deviation. The worst-case expected transmission efficiency of the signal under the variation-aware design for a given standard deviation is defined as the **worst-case expected transmission efficiency under the variation-aware design with a given standard deviation**.

The MRR radii and signal wavelengths from the nominal design are then used to calculate the expected transmission efficiency of signals passing through MRRs affected by a given standard deviation. This means that the configurations obtained from the nominal designs are used to test performance under process variation. The minimum expected transmission efficiency of the signal under the nominal design for a given standard deviation is defined as the **worst-case expected transmission efficiency under the nominal design with a given standard deviation**. It is then calculated and denoted by **"Nom. $\mathbb{E}$"** in Tables 6.2 to 6.4. This is then

compared to the worst-case expected transmission efficiency of the signal from the variation-aware design under the same standard deviation condition, termed **"Opt. $\mathbb{E}$"** in Tables 6.2 – 6.4.

The purpose of this comparison is to determine which design performs better in terms of the expected transmission efficiency of the signal when subjected to different process variations.

6.2. Results Analysis

Upon the completion of the optimization process, the radii of MRRs are categorized for result presentation and analysis. Specifically, radii ranging from 5 μm to 17.5 μm are classified as small radii, denoted by "S-M", and those ranging from 17.525 μm to 30 μm as large radii, denoted by "L-M". The basis for this categorization is that 17.5 units serve as the median radius value.

I also recorded the time required for optimization by both the integer linear programming solver and the simulated annealing algorithm, denoted as "Opt. T.", as well as the time to set the initial solutions, denoted as "Init. T.".

The inputs and results of the integer linear programming model can be found in Table 6.2, and the comprehensive input features and optimization results of the simulated annealing algorithm are presented in Table 6.3 and Table 6.4.

When comparing the optimized expected transmission efficiencies of the simulated annealing algorithm with those of the integer linear programming model under identical topology sizes and standard deviation conditions, it is observed that the difference between them is not significant. In most cases, the simulated annealing approach provides superior optimized expected transmission efficiencies due to the wider range of optimization options available. This implies that the results obtained by applying the simulated annealing algorithm in larger-scale scenarios can be considered credible and reliable.

Table 6.2.: Integer linear programming results under Light and Snake

T	S	$\lvert\mathcal{SP}\rvert$	$\lvert\mathcal{MRR}\rvert$	Init. T.	σ	Nom. $\mathbb{E}$	Opt. $\mathbb{E}$	S-M.	L-M.	Opt. T.
Light	4×3	12	4	0 s	0	**−0.23 dB**		100%	0%	10.43 s
					1 nm	−0.71 dB	−0.71 dB	25%	75%	28.32 s
					2 nm	−1.51 dB	−1.51 dB	25%	75%	12.90 s
					5 nm	−3.6 dB	−3.59 dB	100%	0%	9.82 s
					10 nm	−5.87 dB	−5.84 dB	25%	75%	37.73 s
					0.01%	−1.86 dB	−0.43 dB	100%	0%	5.33 s
					0.02%	−3.52 dB	−0.8 dB	100%	0%	6.43 s
					0.05%	−6.56 dB	−2.12 dB	100%	0%	5.74 s
					0.1%	−9.56 dB	−3.89 dB	100%	0%	3.65 s
Snake	4×4	16	12	0 s	0	**−0.42 dB**		41.7%	58.3%	3919.83 s
					1 nm	−0.92 dB	−0.91 dB	58.3%	41.7%	6776.72 s
					2 nm	−1.73 dB	−1.69 dB	58.3%	41.7%	6828.35 s
					5 nm	−3.85 dB	−3.75 dB	25%	75%	2059.63 s
					10 nm	−6.3 dB	−6.02 dB	25%	75%	2213.59 s
					0.01%	−2.44 dB	−0.72 dB	100%	0%	7247.73 s
					0.02%	−4.28 dB	−1.17 dB	100%	0%	1396.88 s
					0.05%	−7.75 dB	−2.61 dB	100%	0%	1095.46 s
					0.1%	−10.62 dB	−4.62 dB	100%	0%	972.36 s

T: the topology type.
S: the scale of the given topology.
$\lvert\mathcal{SP}\rvert$: the number of signals in the selected topology.
$\lvert\mathcal{MRR}\rvert$: the number of MRRs present in the selected topology.
Init. T.: the time duration for configuring the initial solutions.
σ: the standard deviation.
Nom. $\mathbb{E}$: the value $\mathbb{E}[H_{\text{worst}}]_{\text{dB}}$ optimized under nominal design with the given standard deviation.
Opt. $\mathbb{E}$: the value $\mathbb{E}[H_{\text{worst}}]_{\text{dB}}$ optimized under variation-aware design with the given standard deviation.
S-M.: the proportion of small MRRs.
L-M.: the proportion of large MRRs.
Opt. T. : the optimization time.

6.2.1. Trend of Expected Values

The observations from the experimental results indicate that the worst-case expected transmission efficiency of nominal design and variation-aware designs tends to decrease gradually with increasing standard deviation within the same scale of the same topology. This trend is due to the increasing standard deviation, causing the expected transmission spectrum peaks at the MRR drop port to gradually decrease and broaden. Correspondingly, the troughs at the through port also increase and broaden. As a result, the expected transmission efficiency decreases as the signal passes through the MRR.

Under the same standard deviation condition, the results of both experiments show that as the number of signals and MRRs in the topology increases, the optimized worst-case expectation

Table 6.3.: Simulated annealing results under Light

T	S	$\lvert\mathcal{SP}\rvert$	$\lvert\mathcal{MRR}\rvert$	Init. T.	σ	Nom. $\mathbb{E}$	Opt. $\mathbb{E}$	S-M.	L-M.	Opt. T.
Light	4×3	12	4	2.85 s	0	**−0.23 dB**		75%	25%	31.45 s
					1 nm	−0.77 dB	−0.7 dB	0%	100%	39.54 s
					2 nm	−1.63 dB	−1.49 dB	45%	55%	46.58 s
					5 nm	−3.79 dB	−3.55 dB	25%	75%	39.04 s
					10 nm	−6.09 dB	−5.78 dB	0%	100%	36.44 s
					0.01%	−2.15 dB	−0.4 dB	100%	0%	28.84 s
					0.02%	−3.96 dB	−0.72 dB	100%	0%	36 s
					0.05%	−7.14 dB	−1.93 dB	100%	0%	38.88 s
					0.1%	−9.96 dB	−3.62 dB	100%	0%	46.4 s
	8×7	56	24	19.46 s	0	**−0.85 dB**		45.83%	54.17%	137.62 s
					1 nm	−1.33 dB	−1.37 dB	37.5%	62.5%	138.27 s
					2 nm	−2.16 dB	−2.22 dB	58.33%	41.67%	191.98 s
					5 nm	−4.48 dB	−4.32 dB	41.67%	58.33%	224.12 s
					10 nm	−7.31 dB	−6.87 dB	50%	50%	225.48 s
					0.01%	−2.82 dB	−1.22 dB	100%	0%	213.13 s
					0.02%	−4.7 dB	−1.65 dB	100%	0%	210.06 s
					0.05%	−8.39 dB	−3.21 dB	100%	0%	141.82 s
					0.1%	−11.99 dB	−5.26 dB	100%	0%	226.06 s
	16×15	240	112	119.07 s	0	**−2.87 dB**		41.96%	58.04%	652.6 s
					1 nm	−3.36 dB	−3.61 dB	47.32%	52.68%	997.52 s
					2 nm	−4.32 dB	−4.55 dB	44.64%	55.36%	999.73 s
					5 nm	−7.65 dB	−7.51 dB	41.07%	58.93%	647.31 s
					10 nm	−12.22 dB	−11.73 dB	41.07%	58.93%	669.24 s
					0.01%	−4.91 dB	−4.1 dB	68.75%	31.25%	910.19 s
					0.02%	−7.35 dB	−5.01 dB	89.29%	10.71%	1000.61 s
					0.05%	−12.69 dB	−7.79 dB	97.32%	2.68%	1004.05 s
					0.1%	−17.44 dB	−11.14 dB	98.21%	1.79%	1006.02 s

T: the topology type.
S: the scale of the given topology.
$\lvert\mathcal{SP}\rvert$: the number of signals in the selected topology.
$\lvert\mathcal{MRR}\rvert$: the number of MRRs present in the selected topology.
Init. T.: the average time duration for configuring the initial solutions.
σ: the standard deviation.
Nom. $\mathbb{E}$: the value $\mathbb{E}[H_{\text{worst}}]_{\text{dB}}$ optimized under nominal design with the given standard deviation.
Opt. $\mathbb{E}$: the value $\mathbb{E}[H_{\text{worst}}]_{\text{dB}}$ optimized under variation-aware design with the given standard deviation.
S-M.: the proportion of small MRRs.
L-M.: the proportion of large MRRs.
Opt. T. : the optimization time.

decreases accordingly. This is due to the signal passing through more MRRs, resulting in more insertion loss. When the MRR suffers a process variation, the signal also passes through with more expected insertion loss. This further reduces the expected transmission efficiency of the signal.

Table 6.4.: Simulated annealing results under Snake

T	S	$\lvert\mathcal{SP}\rvert$	$\lvert\mathcal{MRR}\rvert$	Init. T.	σ	Nom. $\mathbb{E}$	Opt. $\mathbb{E}$	S-M.	L-M.	Opt. T.
Snake	4×4	16	12	7.56 s	0	**−0.42 dB**		41.67%	58.33%	88.41 s
					1 nm	−0.97 dB	−0.93 dB	33.33%	66.67%	90.57 s
					2 nm	−1.83 dB	−1.72 dB	41.67%	58.33%	127.51 s
					5 nm	−4 dB	−3.79 dB	33.33%	66.67%	85.2 s
					10 nm	−6.53 dB	−6.08 dB	33.33%	66.67%	95.66 s
					0.01%	−2.47 dB	−0.69 dB	100%	0%	93.96 s
					0.02%	−4.32 dB	−1.04 dB	100%	0%	81.54 s
					0.05%	−7.7 dB	−2.25 dB	100%	0%	104.21 s
					0.1%	−10.85 dB	−4.05 dB	100%	0%	109.11 s
	8×8	64	56	38.89 s	0	**−1.58 dB**		51.79%	48.21%	302.06 s
					1 nm	−2.06 dB	−2.42 dB	35.71%	64.29%	423.6 s
					2 nm	−3.02 dB	−3.3 dB	57.14%	42.86%	432.87 s
					5 nm	−5.84 dB	−6.13 dB	51.79%	48.21%	357.65 s
					10 nm	−9.68 dB	−9.56 dB	53.57%	46.43%	321.28 s
					0.01%	−3.61 dB	−2.18 dB	83.93%	16.07%	504.8 s
					0.02%	−5.59 dB	−3.18 dB	96.43%	3.57%	468.44 s
					0.05%	−10.14 dB	−5.34 dB	100%	100%	484.37 s
					0.1%	−14.61 dB	−8.55 dB	98.21%	1.79%	471.11 s
	16×16	256	240	194.18 s	0	**−6.49 dB**		50%	50%	1565.6 s
					1 nm	−7.16 dB	−6.97 dB	50%	50%	1968.02 s
					2 nm	−8.69 dB	−9.44 dB	50.83%	49.17%	1488.81 s
					5 nm	−14.91 dB	−15.32 dB	48.33%	51.67%	1437.91 s
					10 nm	−20.64 dB	−20.62 dB	46.25%	53.75%	1028.56 s
					0.01%	−8.8 dB	−7.9 dB	57.08%	42.92%	1945.66 s
					0.02%	−11.91 dB	−10.43 dB	64.17%	35.83%	1856.6 s
					0.05%	−20.35 dB	−16.37 dB	60.83%	39.17%	1650.99 s
					0.1%	−26.85 dB	−20.51 dB	65.58%	35.42%	1650.92 s

T: the topology type.
S: the scale of the given topology.
$\lvert\mathcal{SP}\rvert$: the number of signals in the selected topology.
$\lvert\mathcal{MRR}\rvert$: the number of MRRs present in the selected topology.
Init. T.: the average time duration for configuring the initial solutions.
σ: the standard deviation.
Nom. $\mathbb{E}$: the value $\mathbb{E}[H_{\text{worst}}]_{\text{dB}}$ optimized under nominal design with the given standard deviation.
Opt. $\mathbb{E}$: the value $\mathbb{E}[H_{\text{worst}}]_{\text{dB}}$ optimized under variation-aware design with the given standard deviation.
S-M.: the proportion of small MRRs.
L-M.: the proportion of large MRRs.
Opt. T. : the optimization time.

6.2.2. Comparative Analysis

First, I compared the worst-case expected transmission efficiencies under both variation-aware and nominal designs with absolute standard deviations. The worst-case expected transmission efficiencies optimized under variation-aware designs are marginally greater for the small-scale topologies of 4×3 and 4×4. For all other scales, the efficiencies under nominal designs are consistently greater.

In contrast, the worst-case expected transmission efficiencies under variation-aware designs with relative standard deviations are consistently greater than those under nominal designs with the same standard deviations. For the three scale sizes over two topologies, as the relative standard deviation increases, the gap between the worst-case expected values optimized under variation-aware designs and those optimized under nominal designs with the same relative standard deviation also increases.

As visualized in Figure 6.1, as the relative standard deviation increases, the effects of optimization under variation-aware design with relative standard deviation become more pronounced. Specifically, when the relative standard deviation is 0.01%, this difference ranges from 0.81 dB to 1.78 dB; when it is 0.02%, the difference ranges from 1.48 dB to 3.28 dB; when it is 0.05%, the difference ranges from 4.44 dB to 5.45 dB; and when it is 0.1%, the difference ranges from 5.67 dB to 6.8 dB.

It is worth noting that when optimizing under variation-aware design with the relative standard deviation, the tendency is to choose MRRs with small radii. This is because MRRs with small radii exhibit less variation under relative standard deviations, which results in a slower decline in the peak values of their expected transmission spectrum at the drop port. As the network topology expands and the number of signals increases, the proportion of MRRs with large radii selected by the variation-aware design also increases. This is due to the fact that MRRs with large radii offer more resonant wavelengths, thereby accommodating a greater number of signal transmission requirements.

6.2.3. Optimization Time

Only in the Light 4×3 topology is the optimization time for integer linear programming shorter than that for simulated annealing. For topologies larger than Snake 4×4, the integer linear programming model cannot be solved in less than 10 hours. It is worth noting that the integer linear programming model has 38 radius options and 33 wavelength options. There are 1001 radius options, 1001 wavelength options, and larger topologies as the input options for the simulated annealing algorithm. Next, I will provide a detailed analysis of the optimization time for the simulated annealing algorithm.

In the simulated annealing experiment, it takes approximately 34 seconds to generate signal

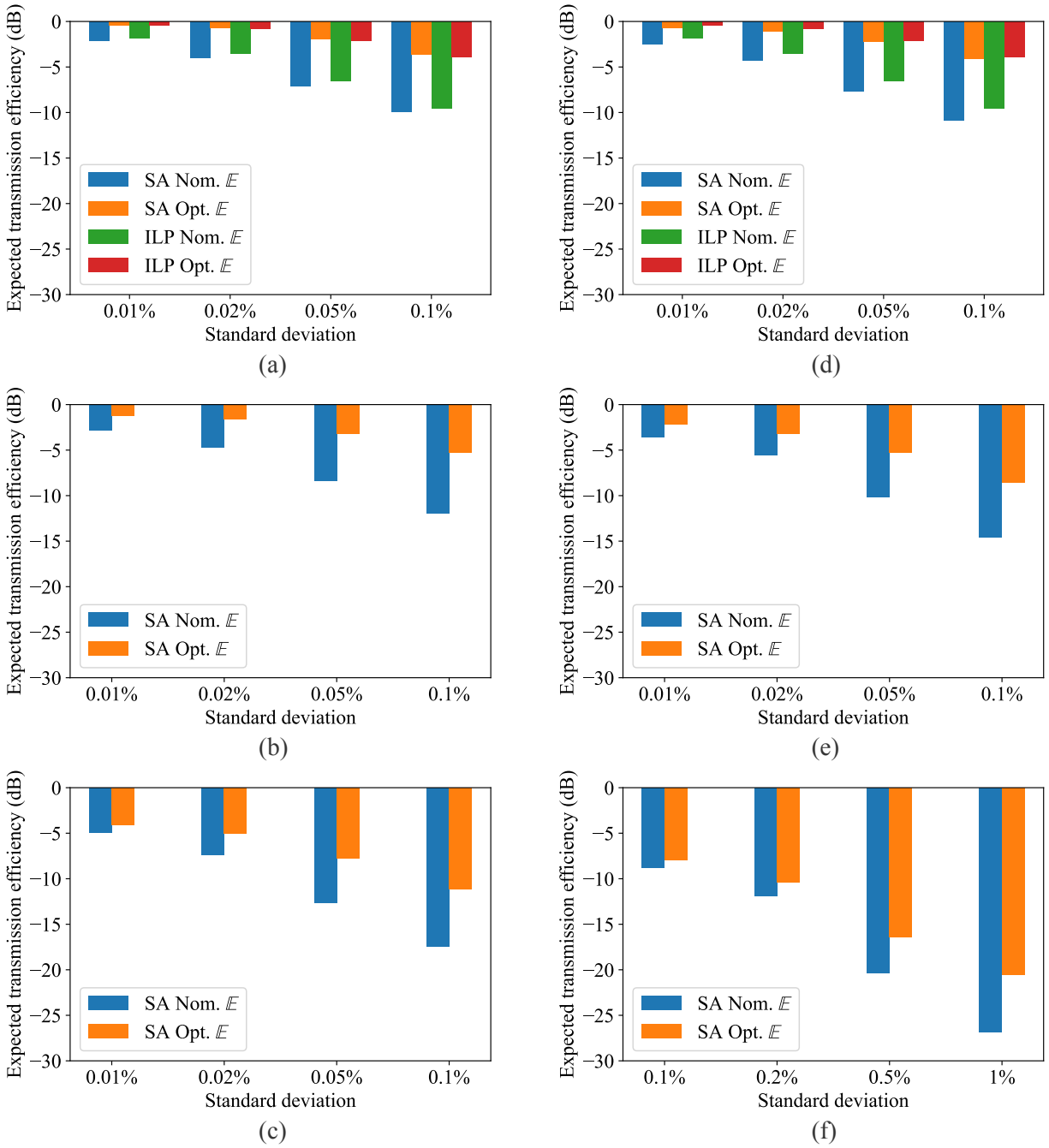

Figure 6.1.: Comparison of worst-case transmission efficiencies optimized under variation-aware design versus those under nominal design with relative standard deviations, using simulated annealing (SA) and integer linear programming (ILP). (a) Light 4×3. (b) Light 8×7. (c) Light 16×15. (d) Snake 4×4. (e) Snake 8×8. (f) Snake 16×16.

transmission efficiency values at both the drop and through ports of the MRR for a total of 1,002,001 data points covering 1,001 wavelengths and 1,001 radius options. It takes approx-

imately 50 hours to calculate the expected transmission efficiency values for these 1,002,001 cases at both the drop and through ports of MRR for eight standard deviations. These are one-time calculations and are not repeated in subsequent steps of the experiment. The time taken to read the pre-stored data is fixed at approximately 37 seconds, with only minor fluctuations within half a second observed across experiments. There is a variation in the time taken to establish the initial solutions for each scale of topology. As the number of signals and MRRs in the network topology increases, the time required to establish the initial solution also increases. This is because the initial radii have to be set for more MRRs. Also, as communication requirements increase, the algorithm requires more wavelength searches to find optimal wavelengths for each communication signal within the given initial solution radii.

For the same network topology and scale size, the time for optimization under nominal design and under variation-aware design show minor differences. As the number of MRRs and signals increases in the network topology, the optimization time increases accordingly. This is because the time to select wavelengths for more signals based on the existing MRR radius configurations increases. Then, given all the radii and existing wavelengths, the algorithm needs to calculate the expected transmission efficiency for more signals and identifies the corresponding worst-case expected transmission efficiency. These processes result in a corresponding increase in optimization time.

In summary, under all circumstances, the optimization time can be controlled within 35 minutes, which confirms that the algorithm can find a design resistant to process variation within an acceptable time.

7. Conclusion and Future Work

In this work, I present a stochastic optimization strategy that, by optimizing the MRR radii parameters and wavelength usage design, maximizes the worst-case expected transmission efficiency of the signal within a given WRONoC topology under process variation conditions. Compared to the optimization results under nominal design, my approach can improve the worst-case expected transmission efficiency of the signal by up to 6.8 dB.

To realize this optimization, I first conducted a comprehensive analysis of the transmission spectrum of MRRs with varying radii related to signals with different wavelengths. Based on this, I built an analytical model using probability theory to accurately calculate the expected transmission efficiency under the influence of process variation. I then constructed an integer linear programming model based on the data generated by the expected transmission efficiency model and validated the effectiveness of this optimization model through a series of small-scale experiments. To expand the scale of optimization and shorten the optimization time, I further developed a simulated annealing algorithm specifically for WRONoC. Experimental results demonstrate the effectiveness of the simulated annealing algorithm in large-scale topologies with millions of design options. These methods enhance the expected transmission efficiency of the signal and thus provide more robustness of WRONoC under process variation.

My future work will extend along the following aspects:

First, I plan to incorporate the consideration of crosstalk into the optimization process. By including the minimization of crosstalk and the improvement of signal-to-noise ratio in the optimization objectives, I expect to further improve the performance and scalability of the network.

Second, I aim to reduce the optimization time. For example, I may consider using heuristic algorithms to generate a good initial solution, which can then be applied to an integer linear programming model for accelerated precise computation.

Finally, I intend to use photonic simulation tools for experimentation to evaluate my design.

Bibliography

Bogaerts, W., De Heyn, P., Van Vaerenbergh, T., De Vos, K., Kumar Selvaraja, S., Claes, T., Dumon, P., Bienstman, P., Van Thourhout, D. & Baets, R. (2012): Silicon microring resonators, Laser & Photonics Reviews **6**(1): 47–73.
https://onlinelibrary.wiley.com/doi/abs/10.1002/lpor.201100017

Brière, M., Girodias, B., Bouchebaba, Y., Nicolescu, G., Mieyeville, F., Gaffiot, F. & O'Connor, I. (2007): System level assessment of an optical noc in an mpsoc platform, Proceedings of the Conference on Design, Automation and Test in Europe, DATE '07, EDA Consortium, San Jose, CA, USA, S. 1084–1089.

Bryc, Włodzimierz (1995): The normal distribution: Characterizations with applications.

Chen, Yu, Xu, Lu, Jiang, Weijun, Wang, Lin, Cui, Shuai, Yu, Yu, Yu, Yuan & Zhang, Xinliang (2022): Silicon based optical all-pass filter, Conference on Lasers and Electro-Optics, Optica Publishing Group, S. JW3B.147.
https://opg.optica.org/abstract.cfm?URI=CLEO_QELS-2022-JW3B.147

Chrostowski, Lukas & Hochberg, Michael (2015): Silicon Photonics Design: From Devices to Systems, Cambridge University Press.

Chuang, Yu-Kai, Zhong, Yong, Cheng, Yi-Hao, Yu, Bo-Yi, Fang, Shao-Yun, Li, Bing & Schlichtmann, Ulf (2021): Robustonoc: Fault-tolerant optical networks-on-chip with path backup and signal reflection, 2021 22nd International Symposium on Quality Electronic Design (ISQED), S. 67–72.

Dekkers, Anton & Aarts, Emile (1991): Global optimization and simulated annealing, Mathematical Programming **50**(1): 367–393.

Durrett, Rick (2019): Probability: Theory and Examples, Cambridge Series in Statistical and Probabilistic Mathematics, 5 Aufl., Cambridge University Press.

Gurobi Optimization, LLC (2023): Gurobi Optimizer Reference Manual.
https://www.gurobi.com

Klenke, Achim (2006): Wahrscheinlichkeitstheorie.

Korte, Bernhard & Vygen, Jens (2012): Combinatorial Optimization: Theory and Algorithms, 5th Aufl., Springer Publishing Company, Incorporated.

Li, Mengchu, Tseng, Tsun-Ming, Bertozzi, Davide, Tala, Mahdi & Schlichtmann, Ulf (2018): Customtopo: A topology generation method for application-specific wavelength-routed optical nocs, 2018 IEEE/ACM International Conference on Computer-Aided Design (ICCAD), S. 1–8.

Li, Mengchu, Tseng, Tsun-Ming, Tala, Mahdi & Schlichtmann, Ulf (2020): Maximizing the communication parallelism for wavelength-routed optical networks-on-chips, 2020 25th Asia and South Pacific Design Automation Conference (ASP-DAC), S. 109–114.

Li, Xia, Shen, Chen, Yu, Xiaohan, Zhang, Yanqiong, Chen, Chao & Zhang, Xiaoxu (2020): Bandwidth-tunable optical filter based on microring resonator and mzi with fano resonance, Bd. 49, S. 1–6.

Meyer, Michael Conrad, Ahmed, Akram Ben, Tanaka, Yuki & Abdallah, Abderazek Ben (2015): On the design of a fault-tolerant photonic network-on-chip, 2015 IEEE International Conference on Systems, Man, and Cybernetics, S. 821–826.

Mirza, Asif, Sunny, Febin, Pasricha, Sudeep & Nikdast, Mahdi (2020): Silicon photonic microring resonators: Design optimization under fabrication non-uniformity, Proceedings of the 23rd Conference on Design, Automation and Test in Europe, DATE '20, EDA Consortium, San Jose, CA, USA, S. 484–489.

Mohammed, Zakriya, Paredes, Bruna & Rasras, Mahmoud (2021): Effect of process parameters on mode conversion in submicron tapered silicon ridge waveguides, Applied Sciences **11**(5). `https://www.mdpi.com/2076-3417/11/5/2366`

Nakagawa, G., Yano, M. & Lee, Y.C. (2001): Optoelectronic packaging technology, in K. J. Buschow, R. W. Cahn, M. C. Flemings, B. Ilschner, E. J. Kramer, S. Mahajan & P. Veyssière (eds), Encyclopedia of Materials: Science and Technology, Elsevier, Oxford, S. 6485–6492.
`https://www.sciencedirect.com/science/article/pii/B0080431526011487`

O'Connor, Ian, Van Thourhout, Dries & Scandurra, Alberto (2012): Wavelength division multiplexed photonic layer on cmos, Proceedings of the 2012 Interconnection Network Architecture: On-Chip, Multi-Chip Workshop, INA-OCMC '12, Association for Computing Machinery, New York, NY, USA, S. 33–36.
`https://doi.org/10.1145/2107763.2107772`

Philip, Peter (2023): Numerical mathematics 1.

Ramini, Luca, Grani, Paolo, Bartolini, Sandro & Bertozzi, Davide (2013): Contrasting wavelength-routed optical noc topologies for power-efficient 3d-stacked multicore processors using physical-layer analysis, Proceedings of the Conference on Design, Automation and Test in Europe, DATE '13, EDA Consortium, San Jose, CA, USA, S. 1589–1594.

Saeed, Ghahramani (2000): Fundamentals of probability with stochastic process.

Selvaraja, Shankar Kumar, Bogaerts, Wim, Dumon, Pieter, Van Thourhout, Dries & Baets, Roel (2010): Subnanometer linewidth uniformity in silicon nanophotonic waveguide devices using cmos fabrication technology, IEEE Journal of Selected Topics in Quantum Electronics **16**(1): 316–324.

Stein, Sheldon H. (2005): Sums and products of jointly distributed random variables: A simplified approach, Journal of Statistics Education **13**(3).
`https://doi.org/10.1080/10691898.2005.11910566`

Tan, Xianfang, Yang, Mei, Zhang, Lei, Jiang, Yingtao & Yang, Jianyi (2011): On a scalable, non-blocking optical router for photonic networks-on-chip designs, 2011 Symposium on Photonics and Optoelectronics (SOPO), S. 1–4.

Truppel, Alexandre, Tseng, Tsun-Ming, Bertozzi, Davide, Alves, José Carlos & Schlichtmann, Ulf (2020): Psion+: Combining logical topology and physical layout optimization for wavelength-routed onocs, IEEE Transactions on Computer-Aided Design of Integrated Circuits and Systems **39**(12): 5197–5210.

Tseng, Tsun-Ming, Truppel, Alexandre, Li, Mengchu, Nikdast, Mahdi & Schlichtmann, Ulf (2019): Wavelength-routed optical nocs: Design and eda — state of the art and future directions: Invited paper, 2019 IEEE/ACM International Conference on Computer-Aided Design (ICCAD), S. 1–6.

Weng, Tsui-Wei, Melati, Daniele, Melloni, Andrea & Daniel, Luca (2017): Stochastic simulation and robust design optimization of integrated photonic filters, Nanophotonics **6**(1): 299–308.
`https://doi.org/10.1515/nanoph-2016-0110`

Xiao, Moyuan, Tsun-Ming & Schlichtmann, Ulf (2022): Crosstalk-aware automatic topology customization and optimization for wavelength-routed optical nocs, IEEE Transactions on Computer-Aided Design of Integrated Circuits and Systems **41**(12): 5261–5274.

Ye, Yaoyao, Duan, Lian, Xu, Jiang, Ouyang, Jin, Hung, Mo Kwai & Xie, Yuan (2009): 3d optical networks-on-chip (noc) for multiprocessor systems-on-chip (mpsoc), 2009 IEEE International Conference on 3D System Integration, S. 1–6.

Zheng, Zhidan, Li, Mengchu, Tseng, Tsun-Ming & Schlichtmann, Ulf (2021): Light: A scalable and efficient wavelength-routed optical networks-on-chip topology, 2021 26th Asia and South Pacific Design Automation Conference (ASP-DAC), S. 568–573.

Eigenständigkeitserklärung

Hiermit versichere ich, dass ich die vorliegende Masterarbeit selbstständig und ohne fremde Hilfe angefertigt, alle benutzten Quellen und Hilfsmittel angegeben und Zitate als solche kenntlich gemacht habe.

Ich versichere ferner, dass ich die Arbeit weder für eine Prüfung an einer weiteren Hochschule noch für eine staatliche Prüfung eingereicht habe.

Ort, Datum Unterschrift